Master Thesis

"From static GNSS positioning to measuring flooding"

Rheinische Friedrich-Wilhelms-Universität Bonn
Faculty of Agriculture
Institute of Geodesy and Geoinformation

Presented by:
Meryem Aydin

Date of Submission:
20 Jun 2022

Supervisor:
Prof. Dr.-Ing. Jürgen Kusche
Makan Karegar, PhD

UNIVERSITÄT BONN

Rheinische
Friedrich-Wilhelms-
Universität Bonn

Institut für Geodäsie und
Geoinformation

Prof. Dr.-Ing. Jürgen Kusche

Professur für
Astronomische, Physikalische
und Mathematische Geodäsie

53115 Bonn
Nussallee 17
kusche@uni-bonn.de

Sekretariat: C. van Eckeren
Tel.: +49(0)228/73-2628
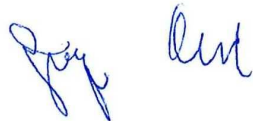Fax: +49(0)228/73-3029
vaneckeren@uni-bonn.de
www.igg.uni-bonn.de

**M.Sc. Geodetic Engineering
Master thesis Task**

„From static GNSS positioning to measuring flooding"

Bonn, 12.11.2021

for Meryem Aydin

Geodetic-quality GNSS instruments measure millimeter-level changes in position of permanent sites for various applications. Among several sources, changes in vertical component of coordinate are attributed to elastic loading and unloading of the crust. Existence of loading signal in GNSS time series has been well-recognised, in particularly with the advent of GRACE satellite by providing global to regional water storage data. However, in low-lying regions and flooding plains where surface runoff and floods are dominant components of water storage variability, the use of GRACE data is still challenging, most probably due to small signal-to-noise ratio. In this thesis, river level data from a dense network in the Mississippi Delta will be used to construct a spatial surface load. Then, elastic half space models and one-dimensional Earth models will be utilized to predict vertical displacement and compare with GNSS time series. The rule of shallow Earth structure will be investigated using half space models. The central idea of this thesis is based on Steckler et al., (2010)'s finding where GPS and river gauge data were used to model Earth deformation from monsoonal flooding in Bangladesh. Based on modeling results, the use of precise GNSS sensor as a means of indirect measure of river level will be investigated.

(J. Kusche)

Abstract

Sea-level rise, coastline erosion, and wetland loss are all caused by coastal subsidence, posing a hazard to coastal people. The Mississippi River Delta (MRD) in the southern United States is a perfect illustration of this. The MRD and the nearby US Gulf Coast are home to a big population, a large amount of economic activity, and crucial ecosystem goods and services. Thus, the region's biggest concern is whether the loss of these wetlands will continue as the world experiences the highest relative sea level rise (RSL).

The global positioning system (GPS) is a space geodetic method that actively observes displacements of continuously operating stations with millimeter (mm) accuracy for numerous applications. Changes in the vertical component of GPS sites allow us to draw different aspects in many areas. According to various sources, vertical land motion (VLM) of stations is attributed to elastic loading. Since 2000, GPS VLM has been used to track seasonal water storage fluctuations. The presence of a loading signal in GPS time series has long been known, especially with the launch of Gravity Recovery and Climate Experiment (GRACE) satellite, which provides global to regional water storage data. The application of GRACE data in low-lying areas and flooding plains, where surface runoff and floods are dominant components of water storage fluctuation, is still difficult.

In this thesis, the comparison of the estimated VLM values and the values obtained from the GPS stations is discussed. Water level data from a dense network of river gauges in the Mississippi Delta are used to construct a spatial surface load with Inverse Distance Weighted (IDW) technique. Elastic half-space model are then used to estimate vertical displacement due to loading. The displacement resulting from the model is then compared with the GPS time series with varying Young's modulus (E). To make a valid comparison, the time series carefully refined from outliers and corrected for the offsets, and the flat-earth approximation rule is used to investigate displacements and potential distortion produced by a point force pressing on the surface of an elastic half-space.

The results reveal that the deformation due by the water loads calculated by the model allows for agreement of displacements in the GPS time series for some stations. The RMS values vary depending on the grid resolution and the magnitude of Young's modulus. For stations MGW3 and LMCN, the best result has an RMS value of 2.6 mm and 3.1 mm . For the $E = 120$ value that gives the best results, the RMS reduction values of the two stations are -11% and 9.9%, respectively. The model is unable to adequately explain the subsidence at all stations. Using alternate Earth model assumptions, experimenting with different interpolation techniques, and precisely correcting offset-related inaccuracies in GPS time series will all be helpful in enhancing the results predicted from the model.

Table of Contents

List of Tables

List of Figures

XIII

XIV

Chapter 1

Introduction

1.1 Motivation

In today's world, coastal areas, which are home to 1.2 billion people and are one of the focal points of economic activities, are still vulnerable to various environmental conditions. It is also widely recognized that the world's coastline is densely populated and human activities along with climate change have unsustainably altered the land used in coastal areas (Nicholls and Small, 2002). One of the most important events that cause coastal deterioration is the changes in water levels. Some of these changes may also show over the deltas, they have seen a period of general expansion over the last few millennia, but increasing relative sea level (RSL) rise and human changes have caused many systems models to deteriorate or fail.

The Mississippi River Delta (MRD), which is located off the coast of Louisiana (Figure 1.1) since 1930, is one of the most notable examples of the rate at which coastal systems are deteriorating. Coastal Louisiana has lost nearly 5,000 km^2 of wetlands in the last century, at rates of up to 100 km^2 each year, and in the face of some of the world's fastest rates of RSL rise, it's uncertain whether the remaining wetlands will be able to survive. To make matters worse, many coastal areas are sinking faster than the waters are rising: natural and human-caused subsidence rates resulting from shallow processes can be 1–2 orders of magnitude higher than the amount of climate-driven sea level rise predicted for the rest of the twenty-first century. (Jankowski et al., 2017). As a result, the elevation changes caused by subsidence must be carefully monitored in both spatial and temporal. Multiple modeling methodologies must be used to predict coastal risks such as storm surges, climate-induced sea level rise, and river flooding in order to assess coastal subsidence.

Figure 1.1: Location of the Mississippi River Delta is illustrated in the figure (Olson and Suski, 2021). Each state and delta region is shown in different colors. Black dots indicate cities in states. The Mississippi river is indicated by a thick dark blue line, while other rivers and waterways that feed and are connected to it are indicated by light and thin blue lines.

In the MRD, precautaions can be taken for natural disasters such as floods or droughts that may occur in the region. In this context, it is critical to track long-term changes in water levels, particularly in this area which. One of the methods of detecting the change in water level is to use river gauge records. Also, GPS VLM has been used to track seasonal changes in water storage since 2000. These improvements have even been applied to water storage in recent years (Nicholls and Small, 2002).

1.2   Aim of the Thesis

The aim of the study, to calculate the deformation of the earth's crust due to water load by using a uniform elastic half-space model. Water level data from river gauge stations in the Mississippi Delta are used to generate a spatial surface load by using Inverse Distance Weighted (IDW) method. Then comparison done between computed displacement from model and observed GPS vertical displacements. Estimated vertical displacement values were modified using different Young's modulus value to find the best fit between the two datasets.

The thesis is structured as follows: The study area is introduced in Chapter 2, in terms of geological formation, climate, and natural disasters that occurs in the region. In Chapter 3, the data used in the study are presented as GPS data and river gauge data, respectively. All used methods and calculations, involving GPS time series offset corrections, mass load inversion to vertical displacements, and validation of results are covered in Chapter 4. The final results and validation findings of the modeling are given and discussed in Chapter 5. The last section Chapter 6 provides an overview about thesis, the challenges encountered during the study, and the contributions that can be made to similar studies in the future.

1.3   Related Works

Geodetic-quality GNSS instruments measure millimeter-level changes in position of continuously operating sites for different applications. The change in the vertical component of these static GNSS measurements is associated with elastic loading and unloading in the earth's crust. This loading effect in GPS time series has been better defined, especially with the launch of the GRACE satellite by providing global to regional water storage data. The usage of Gravity Recovery and Climate Experiment (GRACE) in low-lying areas and flooding plains is still a challenging problem.

The use of river gauge data is one approach to identifying changes in water level. Regarding the studies based on loading detection or in other words, modeling Earth deformation by using water loads, Steckler et al., (2010) which is used GPS and river gauge data to calculate the deformation of earth crust by using elastic half-space model. In this study, different from the thesis, GRACE data is also used. The reason for this, the Ganges, Brahmaputra, and Meghna rivers converge in Bangladesh in a second annual discharge after the Amazon basin. Most of the runoff occurs during the summer monsoon, which causes widespread flooding and the impounded water represents a significant surface load, the effects of which can be observed in GRACE and GPS data. The paper also mention that this region has great advantages for the use of GPS and GRACE datasets, unlike the

Amazon River Basin. Since Bangladesh has one of the world's highest population densities (>1080 people/$km2$), the country's water resources are monitored and controlled through an extensive network of river and groundwater monitoring sites. In the paper, 304 river gauges used to compute water mass. For validation of these data, GRACE water mass equivalents are used. The deformation due to water load is fitted to the GPS stations data with different Young's modulus. The publication also addresses some of the study's limitations. One is to rely solely on river measurement data in the area. The majority of Bangladesh's recharge comes from water imported from rivers, with only 7% coming from local rainfall. Due to the transported water producing local loading, it causes errors in the model as a result of the time lag. Another limitation of this study is that loads from outside Bangladesh are not included. It is also said that if these are included, the spherical earth model assumption would be more appropriate instead of the flat earth approximation. At the end of the study, it is seen that the deflection calculated from the model for different Young's modulus with the GPS vertical component provides good agreement and the RMS value is obtained in mm level.

The knowledge about environmental forces affecting water level variability in coastal waters of the Mississippi River delta makes a great contribution to the evaluation of the results obtained from the thesis. The study, Hiatt et al., (2019), first gives a general information about how the Mississippi delta is formed and then gives place to its historical identity and the climate of the Louisiana coast. Later in the publication, it is mentioned what affects the changes in the water level on the shore. The paper indicates these factors respectively; river flow, tides, atmospheric forcing, human impacts, climate change, and sea level rise. In conclusion, this review provides a detailed summary of the factors affecting water level variability in the MRD region.

At the end of the thesis, constructing a link between water load and vertical land motion is a critical issue. In this context, papers Fok et al., (2020), Fok et al.,(2019), Ji and Herring, (2012), and Ochieng, (2018) are explained the relationship between those datasets mostly in the inverse direction. As mentioned in many sources, surface hydrological processes such as monsoonal rains, droughts, and glacial melting transfer continental water mass and deform the solid Earth below. Space-based geodetic techniques like GRACE and GPS can be used to quantify these changes. In this sense, paper Puskas et al., (2017) evaluated the change in the earth's crust as elastic and poroelastic deformation. Interpreting the elastic deformation part of the study as seasonal, the paper mentions that during the winter or the rainy season there is land subsidence due to more precipitation, and on the contrary, uplift is observed in the earth's crust during the summer and drought periods. As a result, it is observed that the hydrological mass and earth crust have an inverse correlation where the load increases, the earth crust moves downwards, and where the water load decreases, there is an upward movement.

Chapter 2

Study Area

2.1 Overview of the MRD region

Over the past century, the Mississippi delta has gained increasing attention from many geoscientists, biologists, engineers, and environmental planners due to the economic importance of the river and its surroundings to the state of Louisiana and the nation (Olson and Suski, 2021). The MRD is crucial for the region in terms of transportation, industry, human population, and ecosystem services (Coleman et al., 1998). The Mississippi river had also a significant impact on the coastal landforms of Louisiana.

After the most recent rise in sea level about 5,000 years ago, sedimentary deposition of clay, silt, and sand on river banks and adjacent basins formed the modern Mississippi River Delta[1]. The MRD is a river-dominated delta system in North America, supported by the region's greatest system of rivers and tributaries (Olson and Suski, 2021). Each Mississippi River deltaic cycle was a progressive capture of the Mississippi River by a distributary which offered a shorter route to the Gulf of Mexico[1]. The river's dominance over other geological and hydrological processes is reflected in the current bird's foot delta (Figure 2.1). Other factors that contributed to the Mississippi Delta's transformation into a large bird's foot stretching into the Gulf of Mexico include time, weather, and human action[2].

---

[1]The Mississippi River Delta Basin: https://lacoast.gov/new/about/basin_data/mr/default.aspx

[2]Mississippi River Delta:https://earthobservatory.nasa.gov/images/8103/mississippi-river-delta
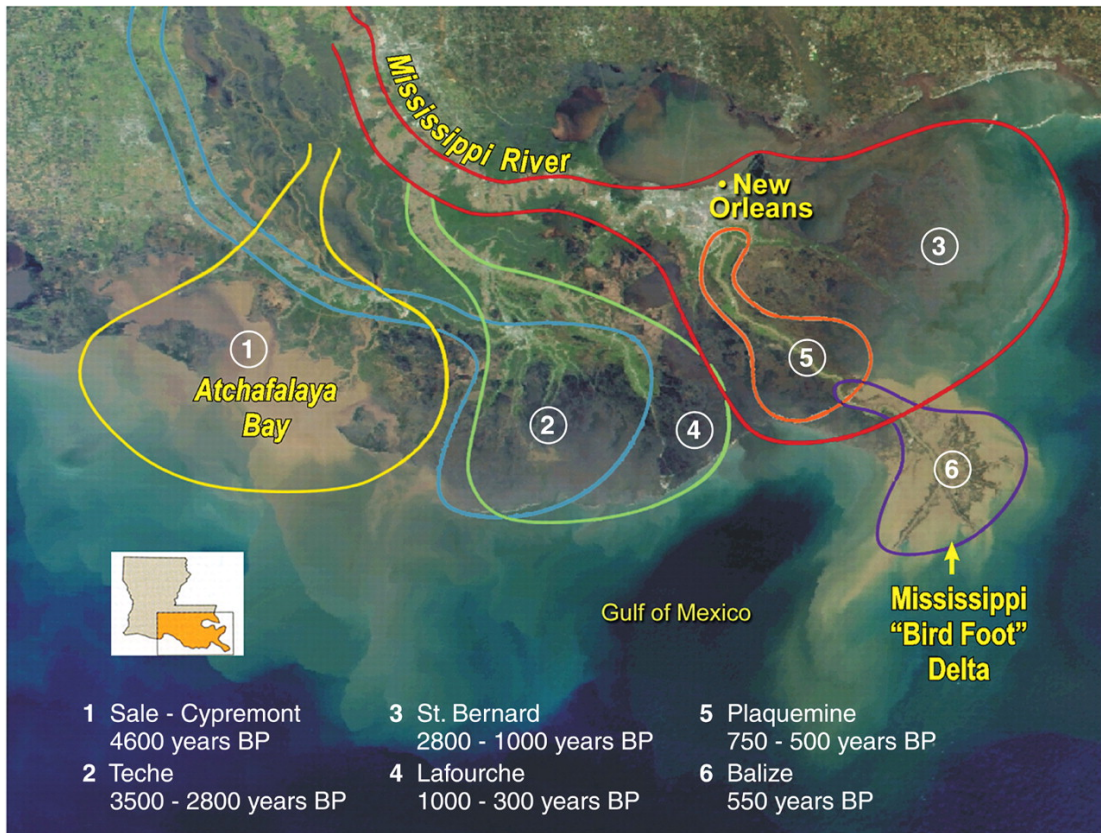
Figure 2.1: The six sub-deltas that form the present Mississippi Deltaic Plain (MDP). The bird foot-shaped delta depicts the importance of the river over other geological and hydrological processes. Currently, about two-thirds of the flow discharged directly into the Bay via the lower Mississippi and one-third via the Atchafalaya River into a shallow bay where a new delta is forming (Day Jr et al., 2007).

However, natural and man-made forces have drastically reduced the delta's sediment load in recent decades. The change over 25-years period becomes clear when comparing two images from NASA Landsat satellites (Figure 2.2)[2]. The river delta faced receding shorelines, flooding, and the addition of some new land which can be seen in Figure 2.3[2] throughout this time. Deltas and wetlands are collapsing as a result of massive oil and gas extraction, and rising sea levels are damaging freshwater vegetation due to saltwater runoff and increase erosion as a result. Currently, a piece of land the size of a football field is lost every half hour according to data from the European Space Agency (ESA)[3].

---

[3] Earth from Space: Mississippi River Delta https://www.esa.int/Applications/Observing_the_Earth/Earth_from_Space_Mississippi_River_Delta

a) June 10, 1976, Landsat 1   b) October 10, 2001, Landsat 7
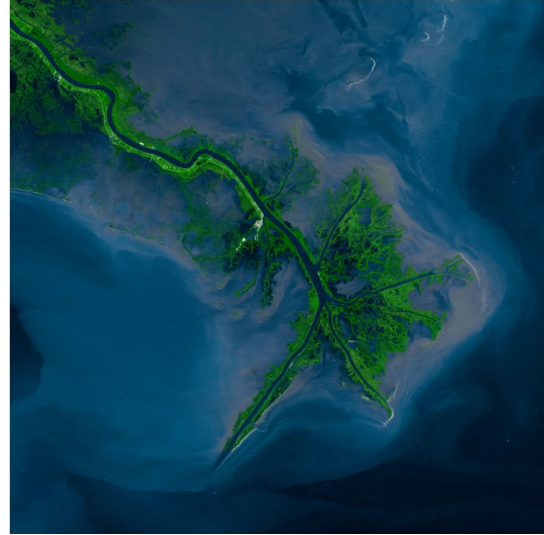
Figure 2.2: Images acquired by (a) Landsat 1 on 10th June 1976, and (b) Landsat 7 on 10th October 2001 to show the changes in the shape of river delta

Figure 2.3: During 25 years of change, the river delta has been beached by retreating shorelines, inundations, and some additional new land.

Many natural disasters continued to strike the delta until today. All natural disasters and extreme events in Mississippi are described in detail in the Section 2.2. Perhaps the most important of these events is Hurricane Katrina, which hit the region in 2005, destroyed most of the wetlands. The issue regarding human management of the Mississippi river heated up in the aftermath of Hurricane Katrina. The river's sediments stabilized the area's subsidence or sinking, to a lower elevation. But the installation of dams stopped the sediment accumulation and also led to the loss of marshes. It is also said that if coastal wetlands had been present during Katrina and earlier hurricanes, the storm may have acted as a flood buffer by delaying the storm's massive waves and absorbing the hurricane and landfall[3].
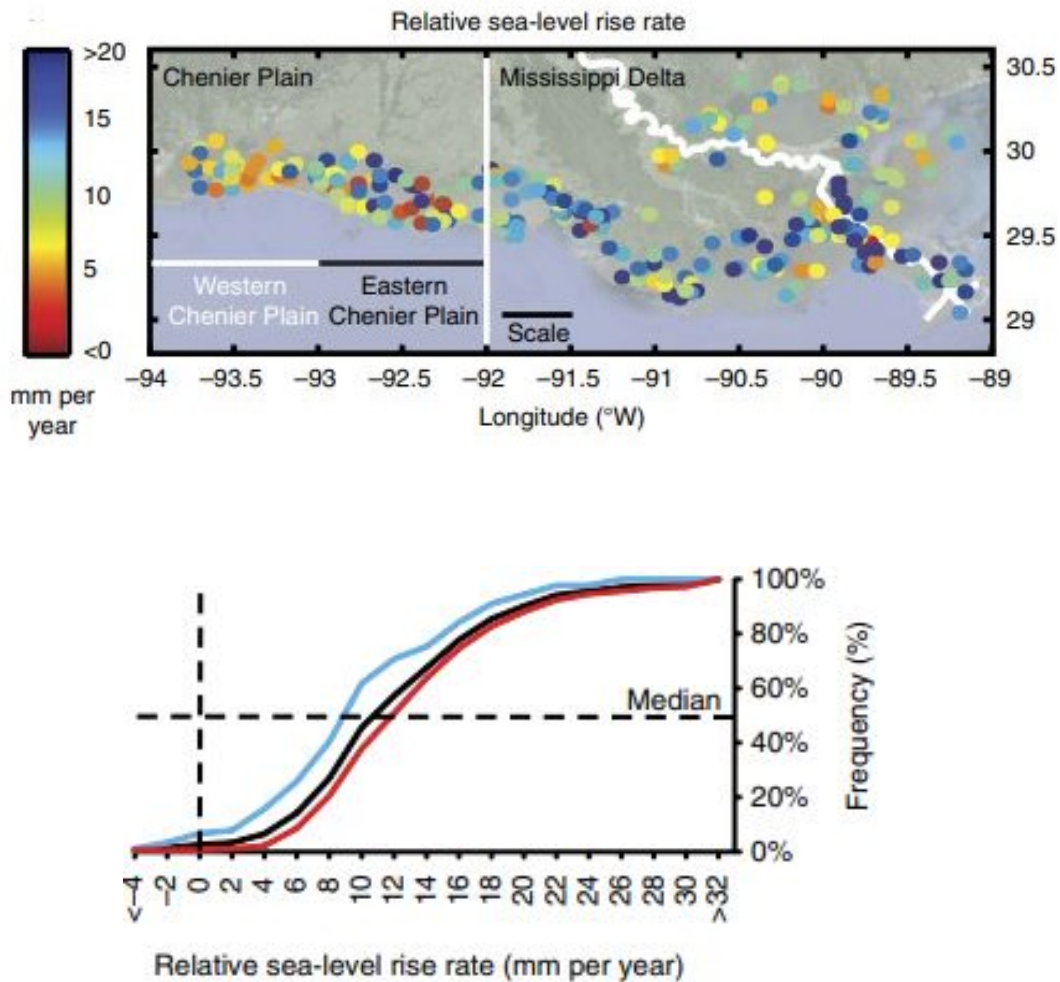
Figure 2.4: The current situation of coastal Louisiana's wetlands is depicted using a spatial pattern and a cumulative frequency distribution. The mean present-day rate of RSL rise given for both overall and in the Mississippi Delta

The major concern for Coastal Louisiana is the massive loss of wetlands (nearly 5,000 square kilometers) over the past century and whether the loss of these wetlands will continue as the world faces the highest RSL rise (12±8 mm per year). The mean present-day rate of RSL is 13.2±8.8 mm per year (Figure 2.4) in the Mississippi Delta (Jankowski et al., 2017), which includes both land subsidence and climate-related sea-level fluctuations (i.e., land ice melting and ocean warming). As a result, the MRD is particularly vulnerable to both catastrophic events (e.g., hurricane-related storm surges) and more chronic environmental degradation such as wetland loss due to a variety of mostly human-caused factors (Day Jr et al., 2007). The region is important in order to better understand and interpret the changes experienced in this sense and to take precautions.

2.2   Mississippi Natural Disasters and Weather Extremes

Over the last few centuries, the Mississippi Delta have lost 25% of their deltaic wetlands area to the ocean (Blum and Roberts, 2009). One of the most important reasons is that there are too many natural disasters happen in Mississippi. According to Federal Emergency Management Agency (FEMA)[4], between 1953 and 2019, Mississippi declared 75 major disasters, with severe storms and hurricanes occurring. Mississippi's most common natural disasters include severe storms, hurricanes, extreme heat and drought, tornadoes, floods, wildfires, winter storms, power outages, landslides, and earthquakes[5]. In this part of the thesis, natural disasters that were important for the region in the past and the damages they caused are given.

Mississippi is situated on the lower reaches of one of the world's greatest river basins. This area receives water from 41% of the contiguous US. The rivers flood to unpredictably high levels during the spring and summer, or when snow melt and heavy precipitation combine. For this reason, especially the coastal areas of the region are under great risk due to flooding (Blum and Roberts, 2009). The Mississippi River Flood of 1927, sometimes known as the Great Flood, was one of the worst floods in state history. This turned out to be the most devastating river flood in the history of the United States. The Mississippi River has

---

[4] Mississippi: https://www.fema.gov/locations/mississippi

[5] Natural Disasters in Mississippi: https://crisisequipped.com/what-natural-disasters-occur-in-mississippi/

reached never-before-seen levels as a result of months of rain. Damage caused by floodwaters in the entire Lower Mississippi River Valley has displaced more than 900,000 people, or about one percent of the total U.S. population (Day et al., 2016).

Due to Mississippi's location and climate, the state also experiences many powerful and destructive storms and hurricanes. From 2000 until the present, at least 28 tropical or subtropical cyclones have impacted the state of Louisiana in the United States. According to David Roth of the Hydrometeorological Prediction Center (HPC), a tropical storm cause landfall along the coast about two times in every three years, and a hurricane makes landfall once every 2.8 years (Roth, 2010). September is the highest month for tropical cyclone activity in Louisiana, with ten total storms, whereas no storms have been reported in the months of December through May. However, the southern portion of the region receives more storm activity than the north (Blum and Roberts, 2009).

Hurricane Katrina, which reached the state in 2005 and killed 1,833 people and inflicted over $100 billion in damage, was the most powerful hurricane that hit the state in terms of barometric pressure. Katrina made landfall as a Category 5 storm at the Louisiana-Mississippi. Following that, Hurricane Rita slammed into the Louisiana-Texas border less than a month later, on September 24, 2005[6].

---

[6] How Hurricanes Katrina and Rita affected the delta: https://mississippiriverdelta.org/our-coastal-crisis/hurricanes/
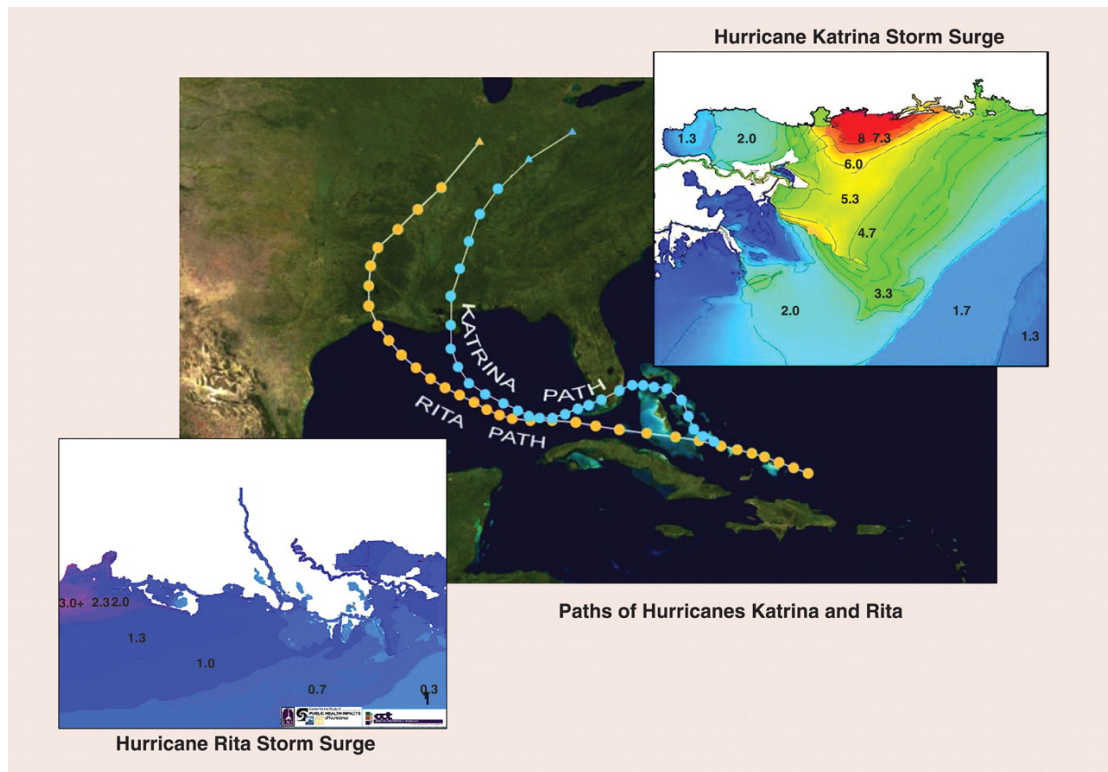
Figure 2.5: The tracks of Hurricanes Katrina and Rita, as well as their surge levels (in meters), inundated regions, levee breakdown sites, and wetland loss, are illustrated in this composite figure (Blum and Roberts, 2009).

Hurricanes Katrina and Rita were the fourth and fifth most powerful storms to strike the MDP since 1893 with respect to maximum wind speed at landfall, but were more remarkable in both cases for the hundreds of kilometers of the coast affected by a storm surge of more than 3m (Blum and Roberts, 2009). The two hurricanes dropped large amounts of rain over large parts of the Mississippi River basin. It could take weeks for heavy rainfall to significantly increase river discharge in Mississippi-sized basins. The Figure 2.6[7] below shows the pattern of rain water deposited on land surfaces. The color scale shows the difference in radar backscatter (in dB) between the present measurement and the mean of the preceding two weeks' data. The backscatter can be calibrated to track changes in surface soil moisture caused by rain. According to the calibration site of Lonoke, Ark, the yellow color correlates to an increase in surface soil moisture of 10% or greater[7].

---

[7] Hurricane Season 2005/Katrina:https://www.nasa.gov/vision/earth/lookingatearth/h2005_katrina.html
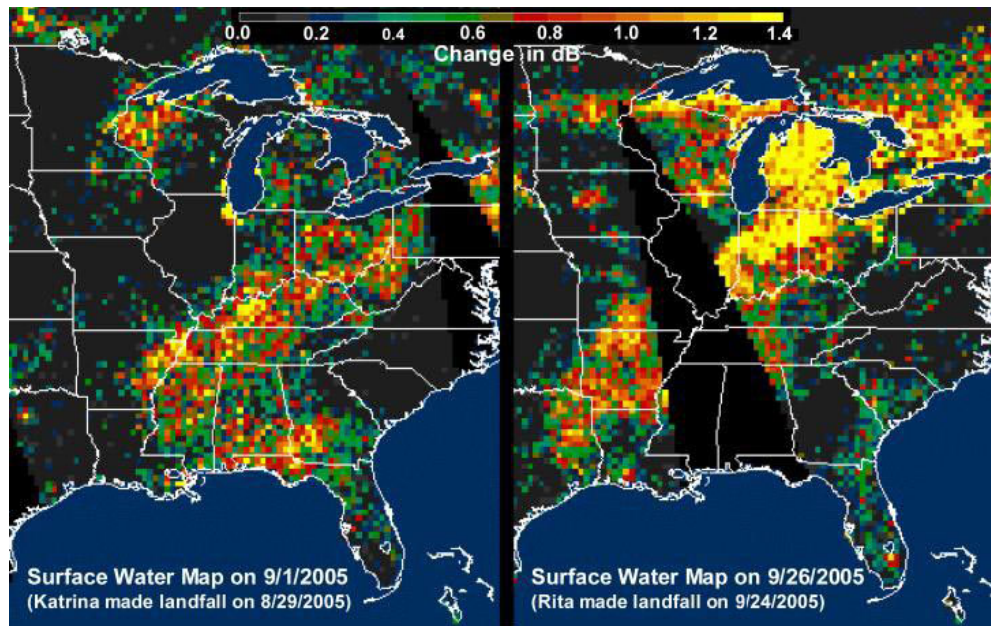
Figure 2.6: Images taken from NASA QuikSCAT satellite data show the massive pattern of rain water deposited on land surfaces by Hurricanes Katrina and Rita throughout different states in the southern and eastern United States.

Another major natural disaster, Hurricane Ida hit the region in November 11, the strongest onshore tropical cyclone during the 2009 Atlantic hurricane season. However, this hurricane should be confused with the 2021 hurricane of the same name, Ida. While the hurricane in 2021 was recorded as Category 4, this hurricane was recorded as a Category 2 hurricane. Numerous flash floods were generated by widespread heavy rains in locations ranging from Mississippi to Maine. Maximum sustained winds at the mouth of the Mississippi River were recorded at 62 mph (100 km/h) and a gust of 74 mph (119 km/h) [8].

In the two-year period 2013 and 2014, damage occurred due to severe storms in the region. Tropical Storm Karen was a system that hit southeastern Pennsylvania and other Mid-Atlantic states in October 2013, bringing record rainfall and flooding. As the storm threatens the Gulf Coast of the United States, National Hurricane Center (NHC) has issued several tropical cyclone warnings and watches, demonstrating the importance of the situation as Karen approaches. On December 23, 2014, a severe tornado occurred in the region. During the day, a strong low pressure formed over southern Texas and moved north into the Mississippi. Over southern Mississippi and southeastern Louisiana, the linked cold front traveled through an unstable air mass, causing scattered thunderstorms. There were a few

---

[8]"Louisiana Event Report: Tropical Storm". National Climatic Data Center, 2010

strong storms, and at least one tornado was reported during the event.

Hurricanes Harvey and Irma, two other major natural disasters, might be first consecutive retired hurricane names since 2005. The Figure below shows the track of two consecutive hurricanes[9]. Hurricane Harvey stalled over Texas from August 25 to August 30, 2017, causing heavy rains, particularly over Houston and the surrounding area on August 26–28. Katrina is also linked to 2017 Hurricane Harvey as the costliest hurricane in the Atlantic basin.
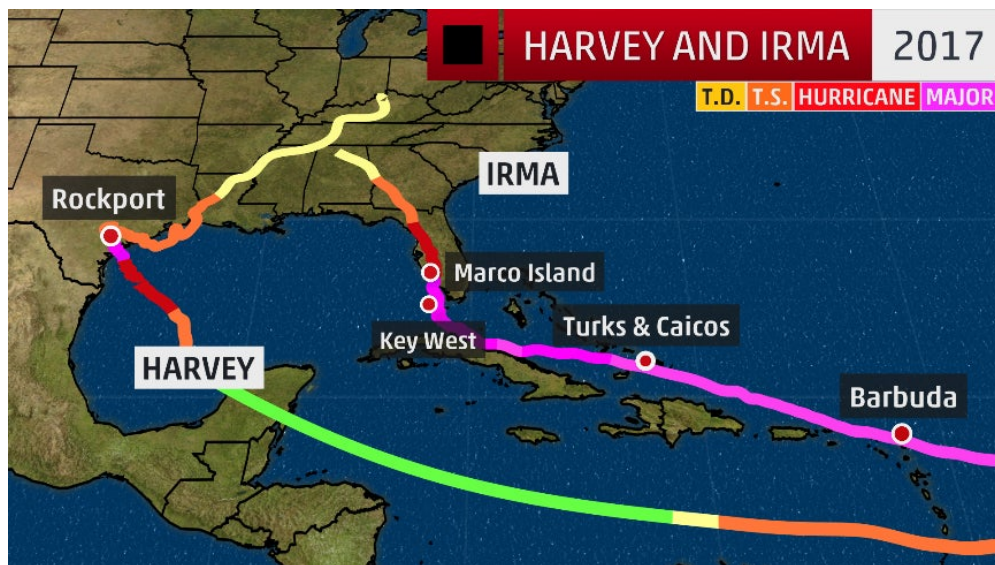
Figure 2.7: The figure shows the path and strength of the two hurricanes in different colors. T.D and T.S stands for Tropical Depression and Tropical Storm, respectively.

Hurricane Irma made landfall in the Florida Keys with 130 mph winds, completing this historic event. It comes just 16 days after Hurricane Harvey roared into Rockport, Texas, with maximum sustained winds of 130 miles per hour. Two Atlantic Category 4 hurricanes make landfall in the United States in the same year for the first time in 166 years of weather records. On the Saffir-Simpson Storm Wind Scale, winds for a Category 4 hurricane range from 130 to 156 mph. Winds of that magnitude have the potential to cause catastrophic damage[10].

─────────────────────

[9] Hurricanes Harvey and Irma: https://weather.com/storms/hurricane/news/ back-to-back-retired-hurricane-names-harvey-irma.

[10] Hurricanes Irma and Harvey Mark the First Time Two Atlantic Category 4 U.S. Landfalls Have Occurred in the Same Year: https://weather.com/storms/hurricane/news/ hurricane-irma-harvey-landfall-category-4-united-states-history
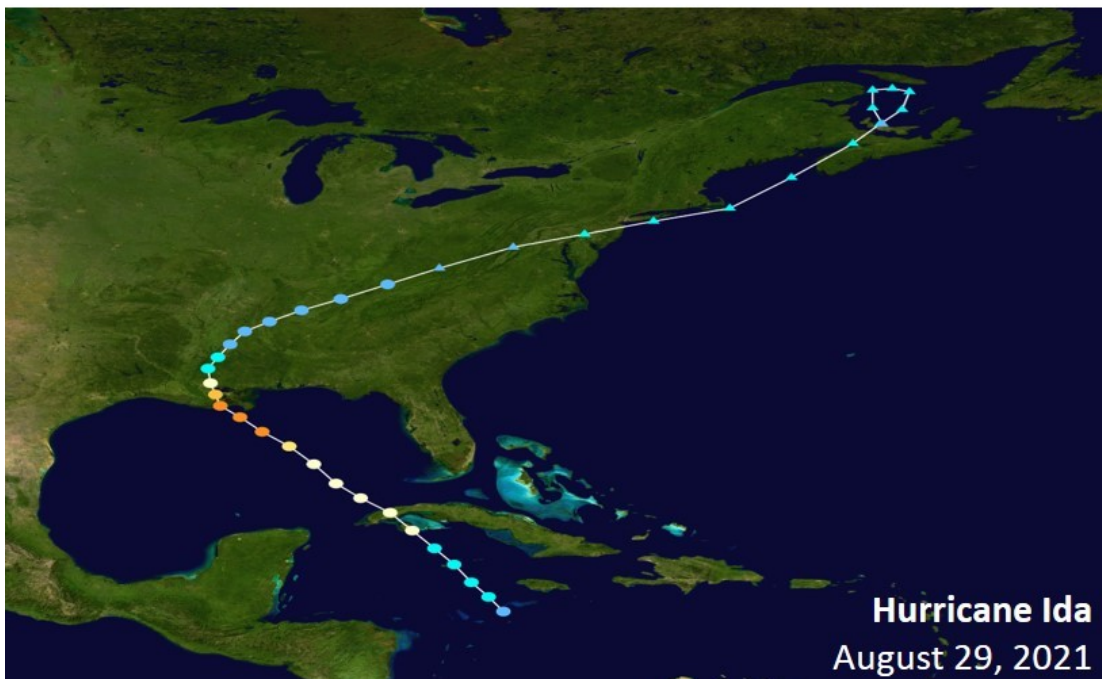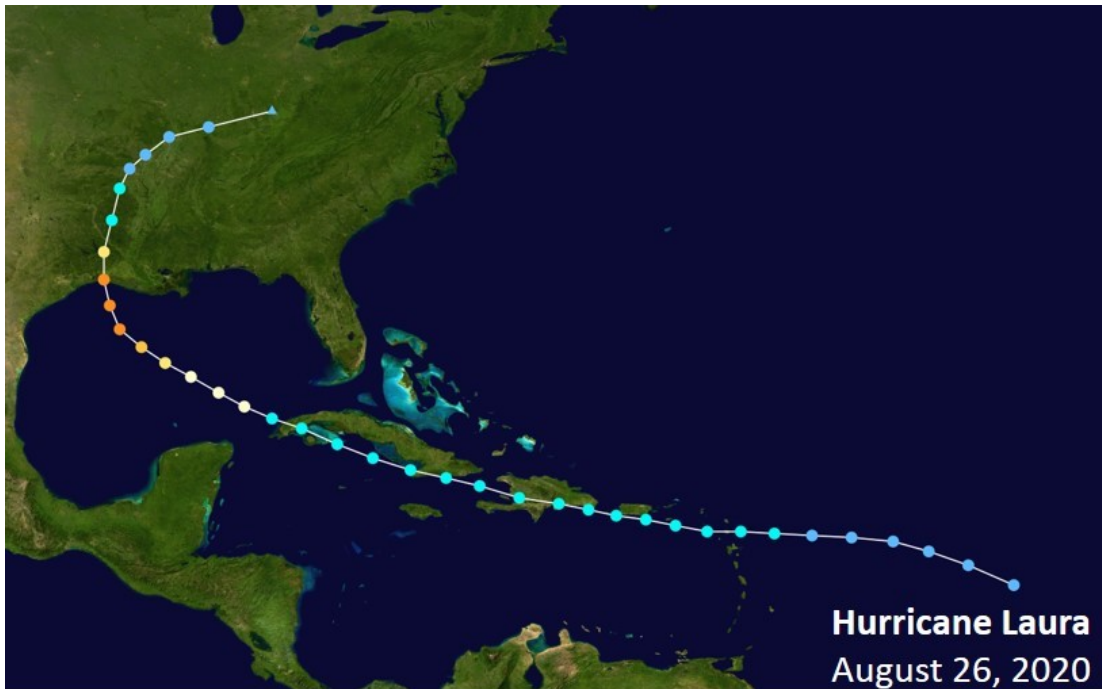
Figure 2.8: The figure shows the storm trace and intensity on the Saffir-Simpson scale for two hurricanes, Laura and Ida. The points represent the storm's location at 6-hour intervals. The storm's maximum sustained wind speeds are shown by the color. The tracking data are taken from National Hurricane Center (NHC).

The 2020 hurricane season set a new record for the most landfall tropical cyclones in a single season, with a total of 5 storms (Roth, 2010). Hurricane Laura formed as a large tropical wave that moved off the West African coast on August 16 and became a tropical depression on August 20. It was the twelfth named storm, fourth hurricane, and first major hurricane of the record-breaking 2020 Atlantic hurricane season.

Widespread severe damage occurred in southwestern Louisiana, with coastal areas experiencing devastating storm surge and inland areas experiencing devastating wind damage. Hurricane Ida was the fifth costliest tropical cyclone recorded in late August 2021 and the fourth costliest Atlantic hurricane in the United States. Ida formed a tie with Hurricane Laura in 2020 and the 1856 Last Island hurricane as the state's most powerful storms ever. It was a deadly and destructive Category 4 Atlantic hurricane that made landfall in Louisiana, becoming the second-most damaging and powerful hurricane on record, behind Hurricane Katrina in 2005. Hurricane Ida, Hurricane Laura (Figure 2.8), and the 1856 Last Island hurricane were the most powerful storms to hit the state in terms of wind speed, with maximum sustained winds of 150 mph (240 km/h), equivalent to Category 4 on the Saffir–Simpson hurricane scale (Roth, 2010).

Chapter 3

Data

The data used in the study are introduced in this part of the thesis. These data are the measurements taken from the available GPS stations situated in the Mississippi River Delta (section 3.1) and the water level measurements acquired from the river gauges to be utilized in modeling part (section 3.2).

3.1 GPS

In the thesis, daily GPS observations provided from the Nevada Geodetic Laboratory (NGL, Blewitt et al., 2018) are used. These coordinate time series are obtained with Precise Point Positioning (PPP) method which resolves phase ambiguity and applies transformation parameters to obtain positions in all directions. Datasets are given in IGS14. This frame is a global, Earth-centered, Earth-fixed, GPS-only implementation of the International Terrestrial Reference Frame 2014 (Altamimi et al., 2016). The coordinate origin of ITRF14 is aligned with the Earth's center of mass. The final products, north, east, and up, and their corresponding sigma and correlation coefficient values are given in tenv3 format for each site. Since this study is about vertical displacements in the earth's crust, only up values are used.

Over the period from 2002 to 2021, a total number of 23 different GPS stations are used in this study. These all continuous GPS stations are situated in the MRD region and their locations are shown in Figure 3.1. The locations of these stations are important for evaluating the correlation of water levels with GPS displacements later in the study (Section B). The operation period of the stations (Figure 3.2) is also another significant parameter for model and GPS comparison in the last section (Chapter 5). The duration of observations of the stations used in the study is seen as at least 5 years and at most 24 years.
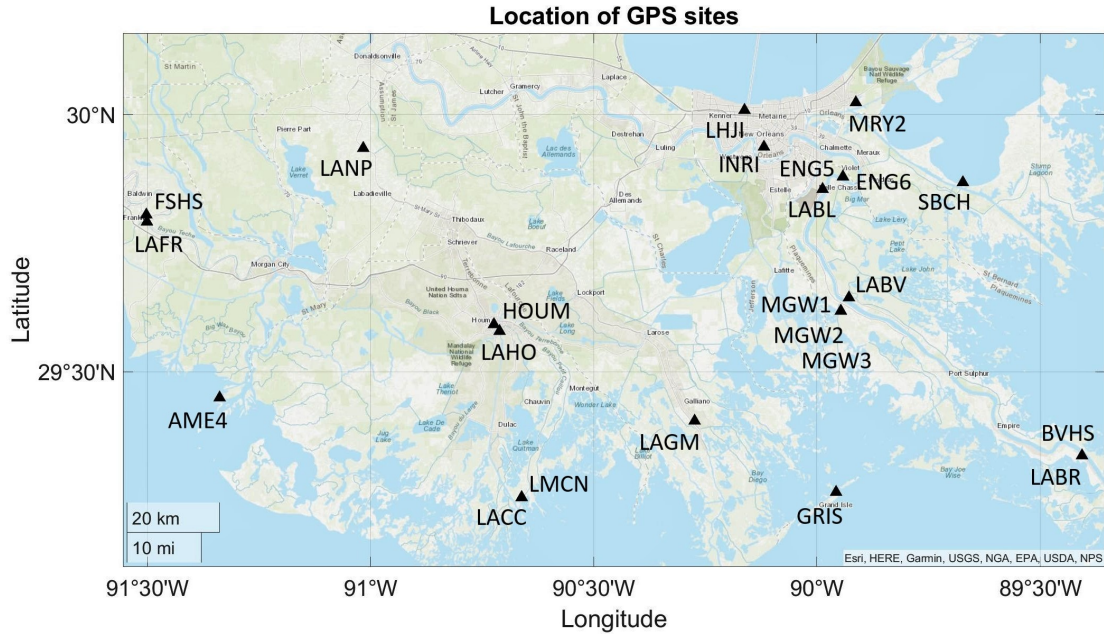
Figure 3.1: Locations of GPS stations in Mississippi River Delta.
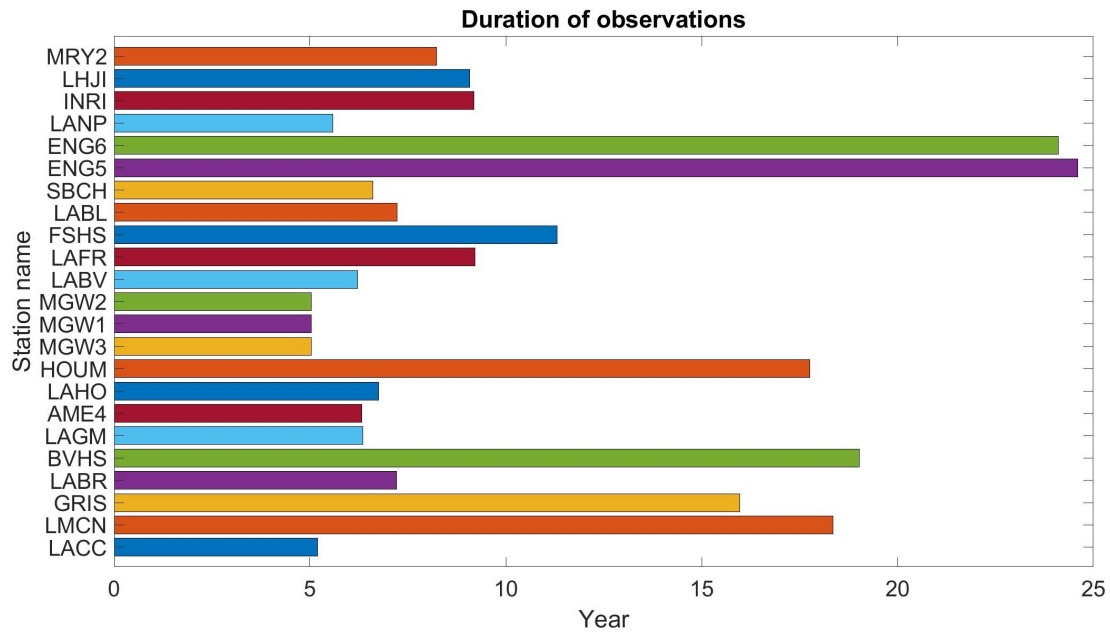
Figure 3.2: Observation period of all 23 station with station names in ascending order of latitude in MRD region.

3.2   River gauge

Spatial and temporal variations in altitude associated with subsidence must be carefully measured. In addition, the contributions of various driving variables must be separated and defined in terms of the total subsidence rate expressed at the land surface.Measurement strategies are especially focused on deltaic areas and coastal megacity "supersites" (Allison et al., 2016).

In this sense, water level measurements in the Mississippi delta are of great importance. Since, subsidence in this delta has been identified as a major driver of rapid wetland loss and degradation of barrier islands, threatening the survival of the coastal ecosystem (Louisiana Coastal Protection and Restoration Authority (LACPRA), 2012). The data from the river gauges used in this thesis is obtained from the Coastwide Reference Monitoring System (CRMS). The CRMS sites are distributed across the entire Louisiana coast, in nine coastal basins and four Coastal Wetlands Planning, Protection, and Restoration Act (CWPPRA) areas. Within a CRMS site[1], there are many CRMS stations or plots. Over the region MRD, 529 river gauge stations are used in this thesis and their location is shown in Figure 3.3.
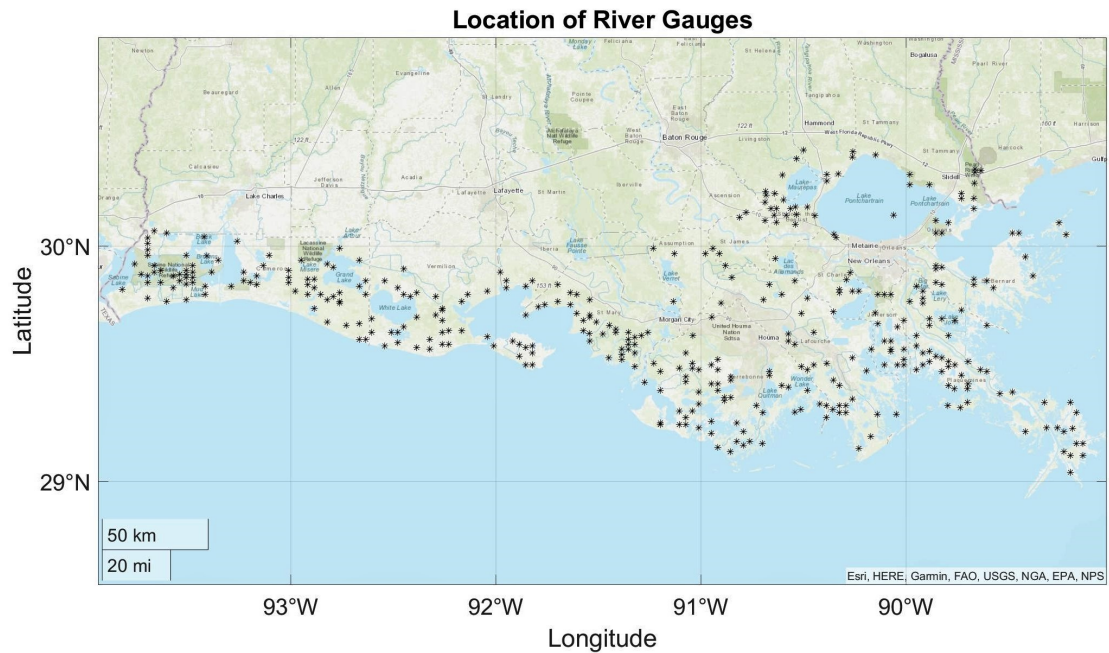
Figure 3.3: Locations of 529 river gauge stations located in the MRD region

---

[1] Coastwide Reference Monitoring System: https://www.lacoast.gov/CRMS/

The users can access the data of the river basin they want by specifying the time interval and selecting the data type on the site. Daily river measurements from the CRMS[1] site are given in feet and datum NAVD88 (North American Vertical Data, 1988). Station names begin with the CRMS's own code and add three more names based on the station's locations. (Table 3.1). In this thesis, all three data types for processes are included and all data has already been provided by the supervisor for the Mississippi River Basin.

Table 3.1: River gauge station names encoding types

Encode type	The location of data recorder
H01	The data recorder is in a bayou or open water body.
M01	The data recorder is in a well in the marsh instead of an open water body.
W01	The data recorder is established in floating marshes where the marsh mat rises and falls with water level.

Chapter 4

Methodology

Chapter 4 describes all methods used in this thesis. First of all, the GPS time series are corrected for offsets. Section 4.1 shows the postprocessing of the data before being used for comparison. These corrections are significant since the datasets are then used to validate the displacements that are derived using the model with the river gauge measurements. The scatter graph between the two data is generated in section 4.2 to illustrate and interpret the relationship between river level and vertical displacement. The water loading that is also the input of the model we used in the study, is calculated in Section 4.3. Finally, Section 4.4, one of the most important parts of the thesis, where we calculate displacement using the forward model.

4.1 GPS Time Series Postprocessing

Vertical displacement estimates obtained from GPS coordinate time series are commonly used to identify and investigate potential geophysical phenomena in specific areas. Consequently, the rate of measured coordinates should be accurately estimated to ensure the correct interpretation of the received GPS signals. However, GPS signal postprocessing is not an easy task due to the challenges in predicting and eliminating all components of existing noise and biases introduced to position estimates. Although the GPS time series used in the study are taken from the NGL website in their pre-corrected form, they still contain systematic effects such as linear trend, harmonic periods, jumps and offsets (Montazeri, 2013). In this thesis, the issue of correcting jumps is discussed in section 4.1.1.

4.1.1 Identifying and Correcting Offsets

Reference frame errors, seasonal fluctuations in GPS signals, the occurrence of jumps and offsets in position data, and antenna phase center model errors are all known to decrease the coordinate and thereby the displacement estimates quality (Montazeri, 2013). In this study, all datasets are corrected in terms of offsets identifying and removing before using vertical displacements from GPS time series for validation. Discontinuities in coordinate time series affect the estimation of site displacements. Therefore, it is crucial to quantify the amplitude of these offsets and subtract them from the time series to get reliable and accurate displacement estimations. These jumps in GPS time series (Figure 4.1a and 4.2a) can be often caused by antenna code, elevation cut off, receiver change or earthquakes.

In this thesis, since the MRD region is tectonically passive, the displacements caused by the earthquakes have quite small effects and they are ignored. A list of potential epochs of discontinuities for GPS stations in the MRD region is obtained from the NGL website[1].

Eliminating offsets from the GPS time series is done by fitting the Heaviside step function $\mathcal{H}$ at the time T_g at which a jump occurs. The discrete form of the step function $\mathcal{H}(t)$ as follows:

$$\mathcal{H}(t) = \begin{cases} 0 & t < T_g \\ 1 & t \geq T_g \end{cases} \tag{4.1}$$

The amplitude of jumps is estimated using the Heaviside step function together with a linear trend through the entire time series (Nikolaidis, 2002). Model equation for each site $y(t)$, can be written as:

$$y(t_i) = a + b(t_i) + c\sin(2\pi t_i) + d\cos(2\pi t_i) + e\sin(4\pi t_i + f\cos(4\pi t_i)$$
$$+ \sum_{j=1}^{n_g} g_j \mathcal{H}(t_i - T_{gj}) + v_i \tag{4.2}$$

where t_i for $i = 1...N$ are the daily solution epochs with units of years, and $\mathcal{H}$ refers to the Heaviside step function. The terms a and b are the site position and linear, respectively. Annual periodic motion is represented by coefficients c and d, while semi-annual motion is described by coefficients e and f. The next term corrects for any number (n_g) of offsets, with magnitudes g and epochs T_g.

---

[1] NGL website/steps: http://geodesy.unr.edu/NGLStationPages/steps.txt

The measurement errors v in the white noise scenario are independent and uniformly distributed, thus it is considered as zero. In this study, the offset epochs are known, the model is linear with respect to the coefficients can be expressed as follows: (Nikolaidis, 2002)

$$x = \begin{bmatrix} a\ b\ c\ d\ e\ f\ \boldsymbol{g} \end{bmatrix}^{T} \tag{4.3}$$

therefore,

$$y = Ax + v \tag{4.4}$$

where A is the design matrix of partial derivatives.

The unweighted least squares solution for the best linear estimates of the unknown parameters $\hat{x}$ is described as:

$$\hat{x} = (A^{T}A)^{-1}A^{T}y \tag{4.5}$$

with parameter covariance

$$C_x = x^2(A^{T}P^{-1}A)^{-1} \tag{4.6}$$

and the residual vector v becomes,

$$\hat{v} = y - A\hat{x} \tag{4.7}$$

GPS time series corrected according to steps taken from NGL website still contained jumps. Therefore, it was deemed necessary to make manual offset corrections for some stations. Otherwise, these uncorrected large jumps could have caused the long-term trend of the time series. It can be seen in Figure 4.1b and 4.2b that after the corrections the jumps or outliers are no longer avaliable for given two GPS sites. The displacement values shown in the figures represent deviations in cm from the reference date. January 1, 2020, which is the common date for all stations, has been chosen as a reference.
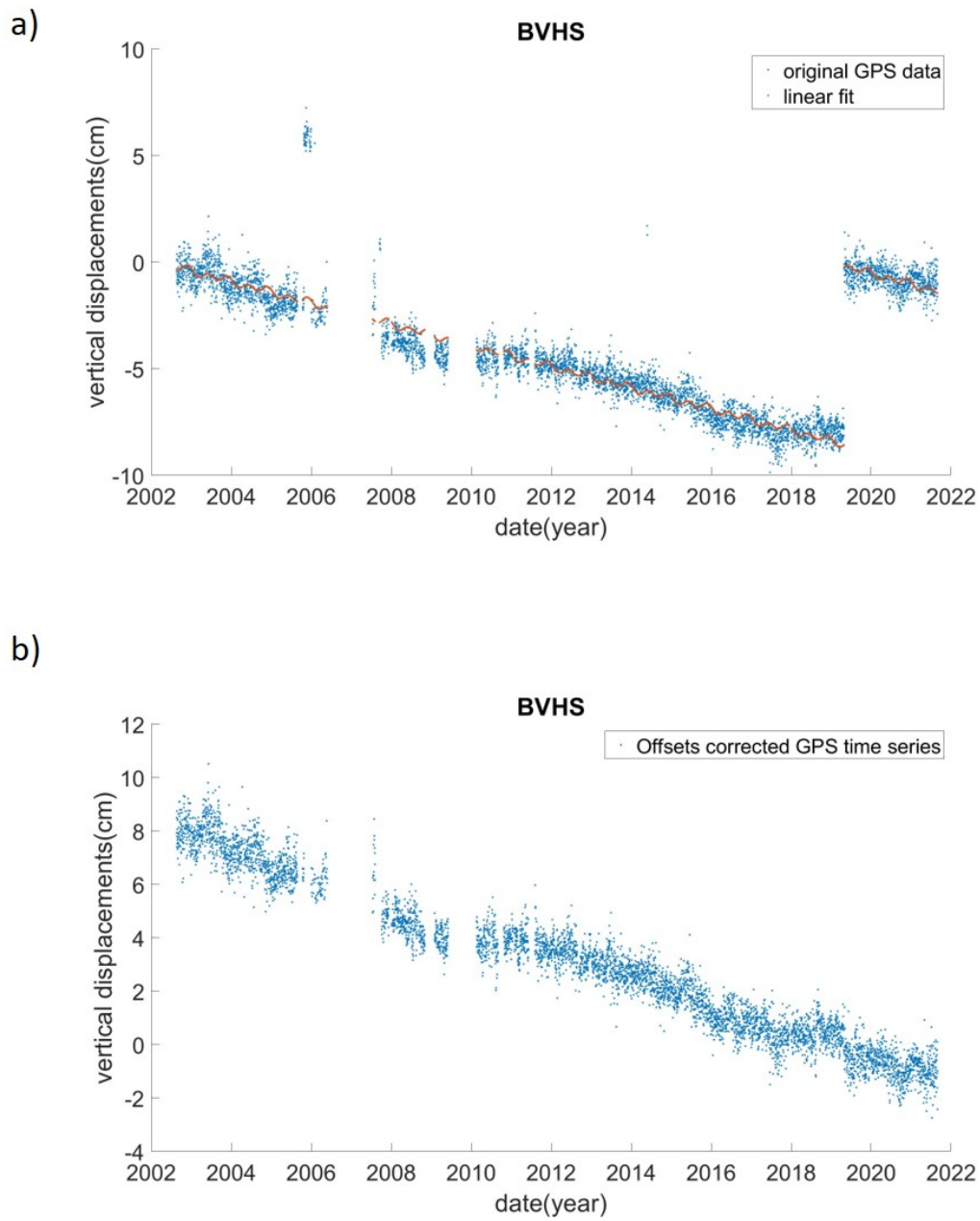
a)

b)

Figure 4.1: (a) The original GPS time series and its linear trend are shown as orange line, (b) the corrected time series after removing outliers
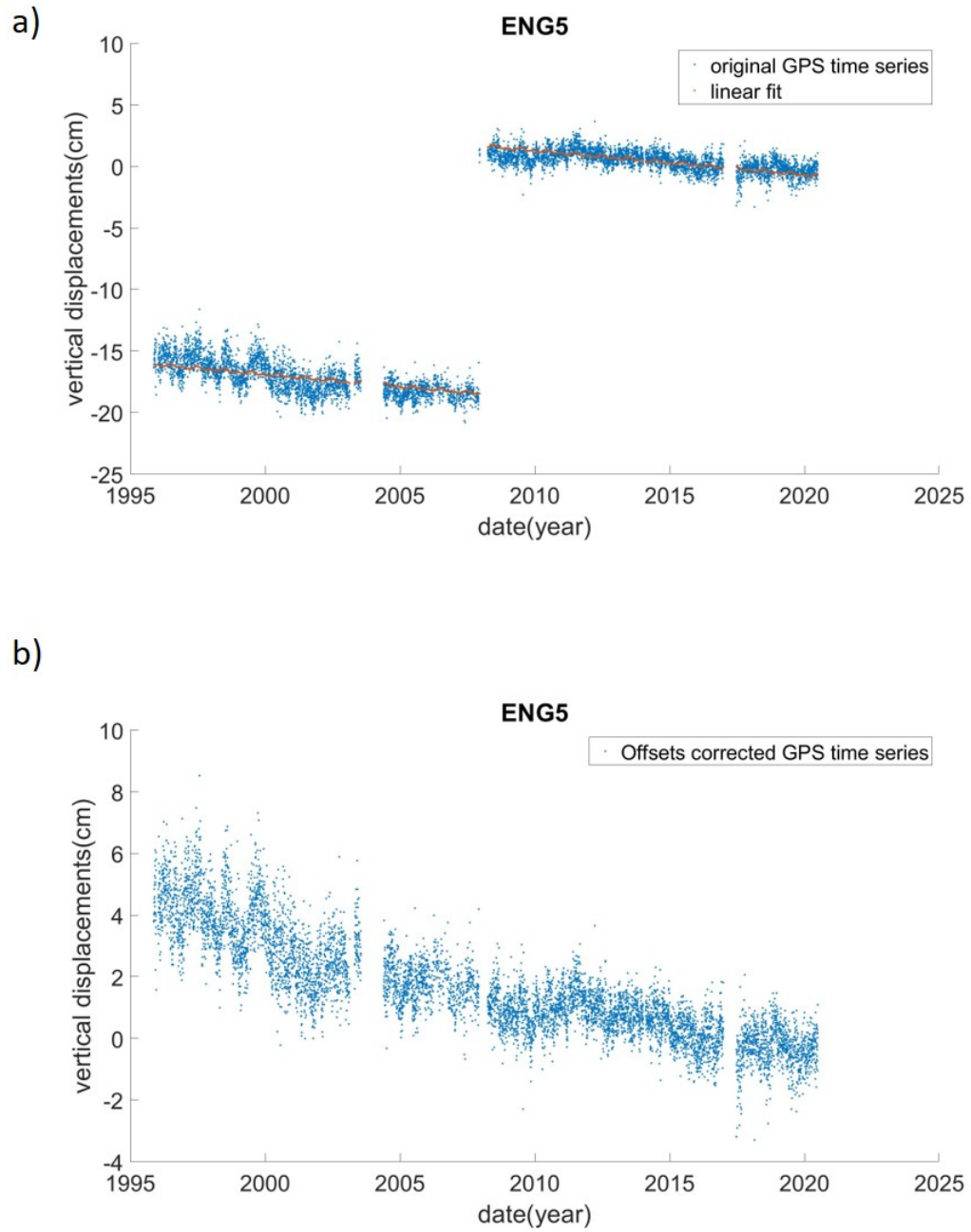
Figure 4.2: (a) The original GPS time series and its linear trend are shown as orange line, (b) the corrected time series after removing outliers

4.2 Relationship between water level and VLM

The natural processes of vertical land motion (VLM) lead to globally variable rates of subsidence (downward VLM) and uplift (upward VLM). These natural processes such as tectonic, glacial isostatic adjustment and sediment compression, as well as anthropogenic processes such as fluid extraction, are important because they are key physical processes that drive vertical land movement in coastal areas (Shirzaei et al., 2021). For the twenty-first century, steady and relatively low rates of subsidence and uplift due to tectonic processes and glacial isostatic adjustment can be assumed. On the other hand, compaction associated with sediment loading and fluid extraction, as well as large earthquakes, cause substantially higher and variable subsidence rates.

In this part of the study, correlation analysis was performed to understand and interpret the relationship between the water level change in the MRD region and the change in the vertical positions of the GPS stations. This analysis was based on a measured correlation coefficient as a statistic known, which expresses the degree of a relationship and its value ranges between -1 and 1 (Ochieng, 2018). After the calculations, it was expected to obtain a negative correlation between the variables, in other words, where the water level increases, there is land subsidence caused by sediment compaction. The degree of correlation was studied using the scatter diagram. However, before making these scatter plots, weekly and monthly temporal averaging was performed in Section 4.2.1 for both datasets which are GPS displacements and water level values from river gauges, since the scatter of the datasets is still characterized by errors and seasonal trends (J. Li et al., 2000). The last Section 4.2.2 deals with the representation of correlation values on a map of the region, primarily for visual interpretation.

4.2.1 Temporal Averaging

In this section, temporal averaging was performed with different window sizes for both data sets to understand the evolution of regional hydrological mass, since daily time series are challenging to resolve hydrologic events. Before the averaging process, the datasets were detrended. The reason for this process is to remove an aspect from the data that is causing some kind of distortion in order to see subtrends.

The distance factor was taken into account before determining the relationship between the detrended data sets. The relationships between stations that are close to each other, as is well known, produce clearer results and most of the load effect comes from the water closest to the observation site. As the distance decreases, the correlation between them is expected to increase. In this study, there are 23 GPS stations and 579 river gauge stations, and to better understand the relationship between distance and correlation, a buffer was applied to identify

the corresponding river measurement stations for each GPS station. The buffer was set at 20 km so that at least one river gauge station could correspond to each GPS station.When viewed by removing this buffer, it is understood that the relationship between the distance and the correlation values is significant within 100 km of the interval. In other words, the correlation relationship between GPS stations and river gauges is not significant after 100 km. It is possible to clearly see from the figure that there is a correlation between them within this range.
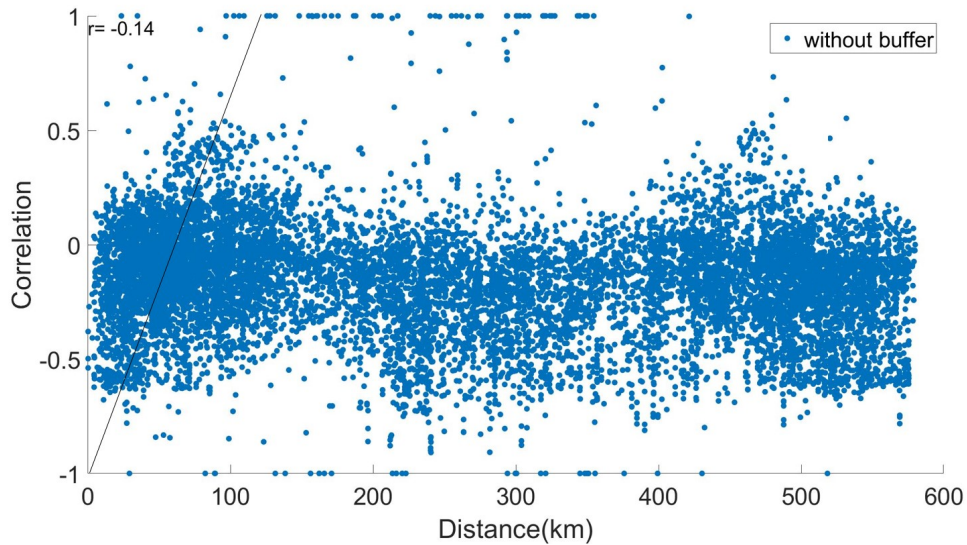
Figure 4.3: Scatter diagram between distance and correlation value. Within the 100 km correlation and distance values has a relationship and it is defined as a black line. Distance between GPS sites and river gauges is defined as km. From the figure, it is also possible to see that the correlation relationship is negative as the distance decreases.

Afterward, the detrended data averaged as weekly, bi-weekly, 3-weekly, and monthly. The correlation between these averaged datasets was obtained with the Pearson Correlation principle. The square of Pearson's Correlation, often known as the Coefficient of Determination (R2), is a straightforward way of evaluating the value of the correlation coefficient. In this study, The expectation was to obtain a negative correlation between the two variables where land subsidence, or rather vertical displacements, occurs while the water level rises. In order to see the distribution of the calculated correlations for the different window sizes, the histograms shown below (Figure 4.4) were created for each scenario.
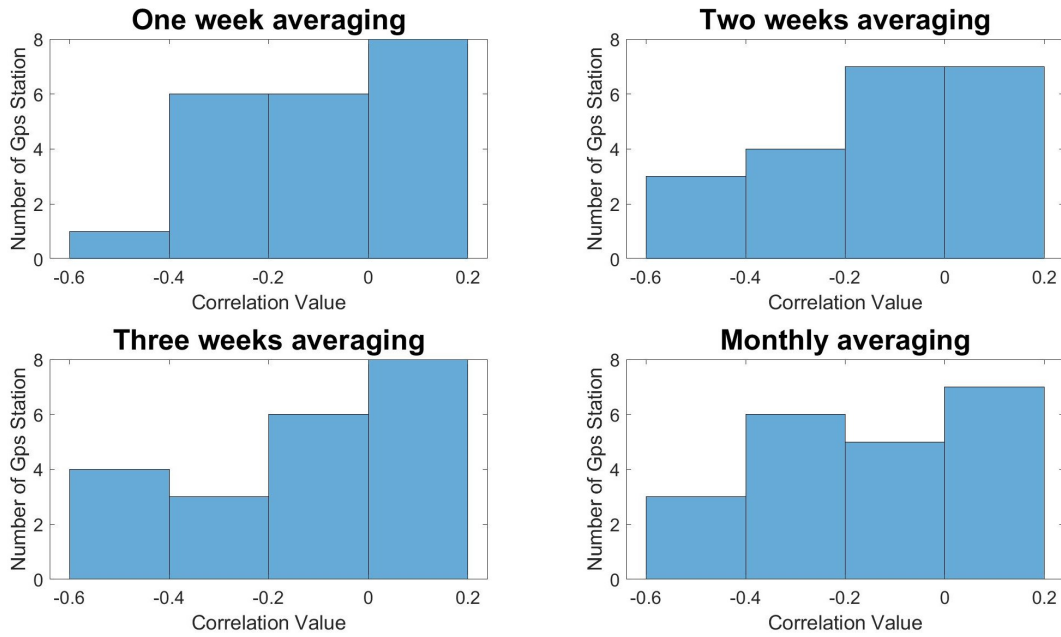
Figure 4.4: Histogram shows distributions according to different temporal averaging scenarios. There is an increase in the tendency to show a negative correlation towards the monthly mean.

The primary goal of this procedure is to remove an aspect of the data that is creating some type of distortion so that subtrends can be seen. Detrended and temporally averaged two datasets are shown as a scatter diagram to see the correlation between them within a buffer of 20 km.

It is clearly seen that the detrended and monthly averaged time series of both datasets show more negative correlation than other averaging scenarios. This study from scatter diagrams expects to get a negative correlation since water level increases, it causes deflection on Earth's surface in a downward direction and it is basically called subsidence. It means if the correlation between two datasets is close to -1 represents a higher subsidence rate. The correlation between variables also can be related to the distance. Since it is thought that the similarity between two variables increases as the distance between them decreases, the correlation between them is expected to increase as well. Section 4.2.2 has also been studied to deduce this assumption. This section has been introduced specifically to visually interpret this relationship.
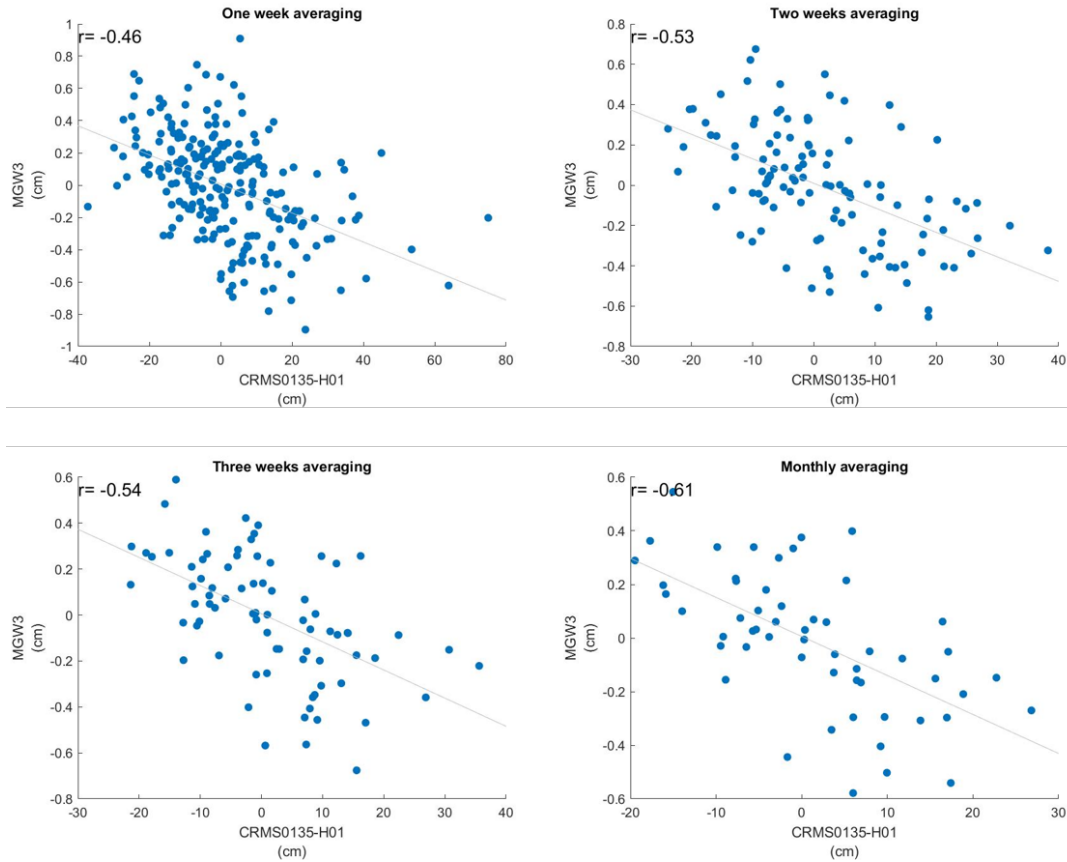
Figure 4.5: Scatter diagrams for different temporal averaging scenarios. monthly averaged time series exhibit stronger negative correlation than other averaging scenarios.

To better understand the importance of averaging, scatter diagrams for different temporal averaging windows are shown in the Figure 4.5 for station MGW3. It shows its relationship with one of the closest river gauges in the buffer.It is seen that the negative correlation value approaches -1 as the averaging window increases. In order to better understand the distance and correlation relationship, the locations of the stations and the surrounding river gauges on the map are shown in the next section (4.2.2).

4.2.2 Geobubble plots

The correlation analysis between water level changes and GPS vertical displacement is a key element of this study. In this section, further investigation is made to get a more specific link between these two datasets. Since it was thought that showing this relationship on the map would lead to a better visual interpretation, GPS stations and the corresponding river gauge stations in the specified buffer were displayed on the map with their correlation values and distance information.

Figure 4.6: Negative correlation between MGW3 station and corresponding river gauges within the buffer 20km are shown with bubbles. The black triangle represent location of the GPS station.

In the study, 12 of the GPS stations showed only negative correlation with the river gauge stations around, 10 of them both positive and negative and only one of them showed positive correlation. The change in color of the bubble represents the distance, while the size of the bubble reflects the correlation size for all the station. The negative correlation values shown in the figure should be considered as minus signs. One of the negatively correlated stations, MGW3, is shown in Figure 4.6 above. As can be seen from the map, this station is located right next to the Mississippi River. It has an inverse correlation with 22 river gauge stations in the buffer. The closest river gauge station is about 300 meters away and the correlation value with this station is -0.539. While the highest correlation value was -0.645, the lowest correlation value was -0.433 at a station 10 km away from itself.
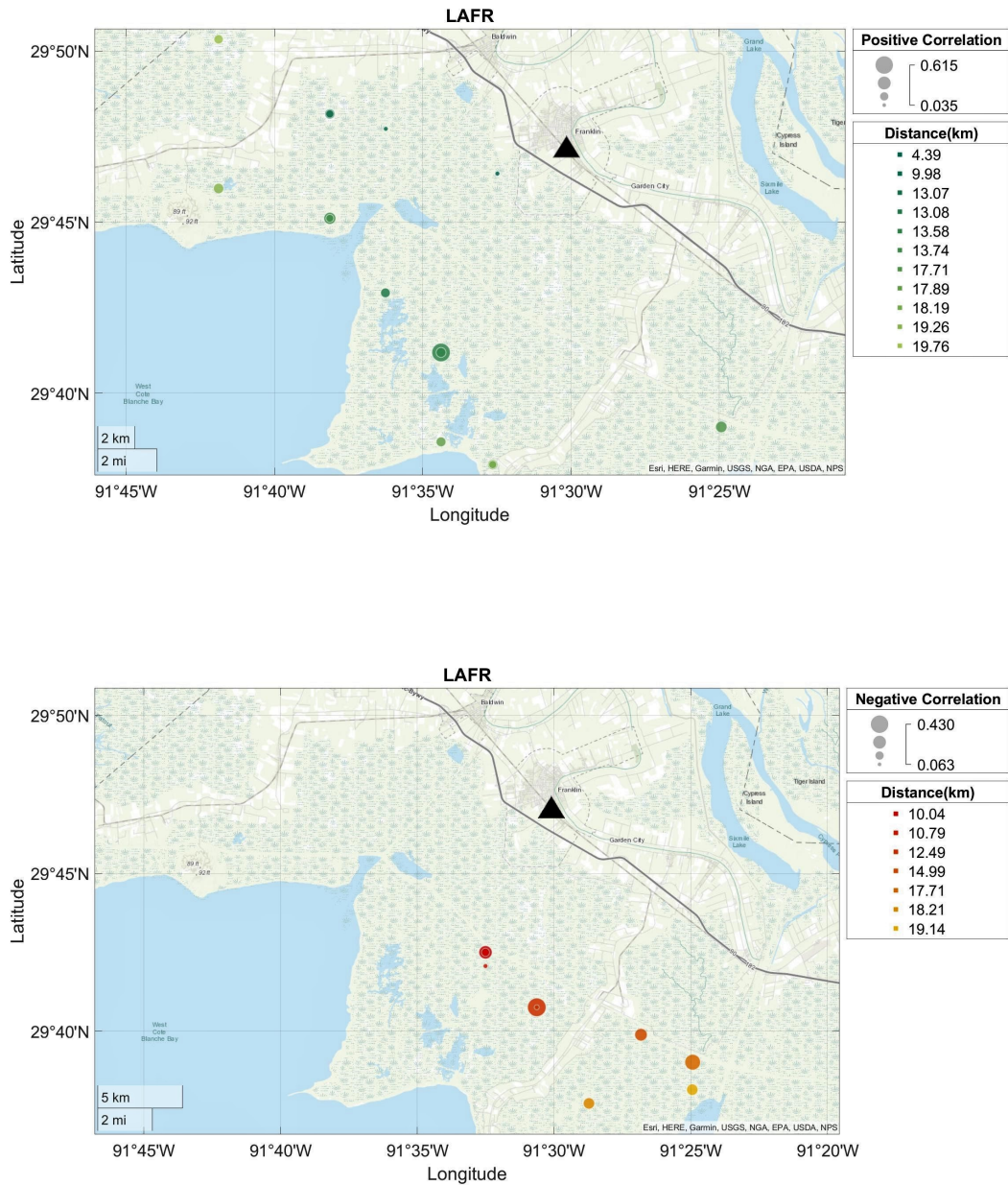
Figure 4.7: Positive and negative correlation between LAFR station and corresponding river gauges within the buffer 20km are shown with bubbles. The black triangle represent location of the GPS station.

The LAFR station correlated both negatively and positively with the corresponding 25 river gauge stations within the buffer. Green scaling bubbles show positive correlation values, while red scaling bubbles show negative correlation. It should be noted that the LAFR station's location is not located right next to the Mississippi

river like MGW3.The station obtained the highest negative correlation value of -0.430 with a station 10 km away from it. The station showed the highest positive correlation value of 0.615 with a station almost 14 km away from itself.
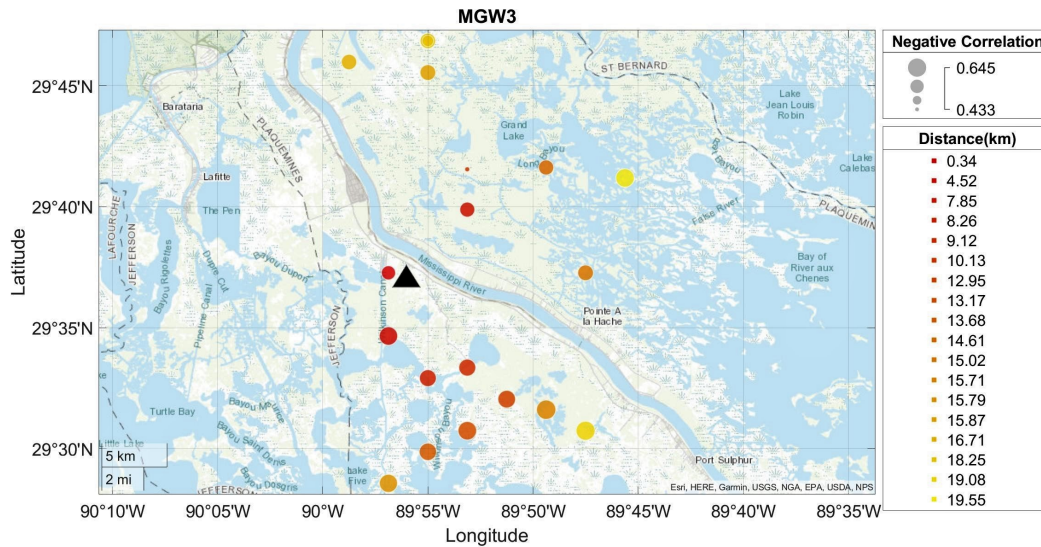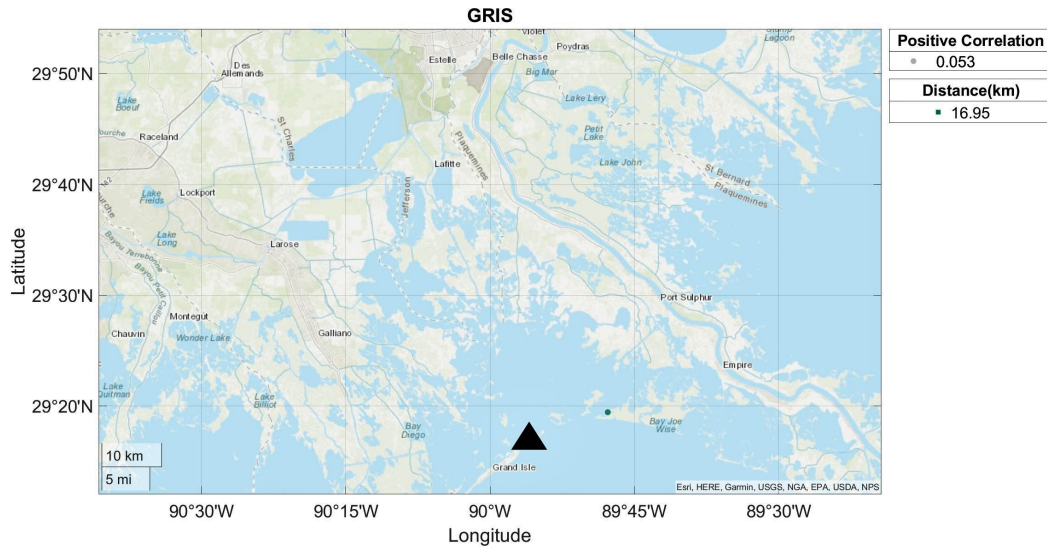

Figure 4.8: Positive correlation between GRIS station and corresponding river gauges within the buffer 20km are shown with bubbles.The black triangle represent location of the GPS station.

The last example, the GRIS station, showed a positive correlation with only one river gauge station in the determined buffer. There is a positive correlation with a value of 0.053 with the station, which is approximately 17 km away from it. Since there are not many river gauges used in the study near the station due to its location, it would not be correct to evaluate the relationship between water level and GPS displacement through this example.

Considering the examples shown in this section, it would not be wrong to say that there is a negative correlation between water level and GPS vertical displacements. This means that where the water level rises, a subsidence due to mass loading can be seen. However, this change does not mean that it will always be downwards, since some stations show a positive correlation, which means that it would not be correct to directly associate the uplift or subsidence seen in the GPS station with the water level change. It would be correct to make a comment by considering the factors affecting the relationship between these two changes.

4.3   Mass load calculation

The areas where water is stored on earth are many such as oceans, lakes, rivers, soil, etc. In continental interiors, groundwater and surface waters come predominantly. These water mass changes seasonally and is sufficient to induce GPS time series displacements of several millimeters. Water is stored in these storage media when there is more precipitation during the winter or rainy season. The weight of the excess water applies pressure on the ground surface, which response to the load by deforming elastically. When evaporation and runoff outpace precipitation during the summer or dry season, surface water mass decreases, and the ground rebounds, causing uplift (Puskas et al., 2017). Thus, elastic deformation due to the water mass changes at the Earth's surface from water bodies is a crucial task. In this part of the study, the water loading is calculated to compare this displacements in the GPS time series with the model results.

The spatial interpolation technique for detrended and monthly averaged water level data is explained to be used later in the Forward modeling, which is the last part of the methodology section. The main reason to use spatial interpolation methods is to estimate water level in unmeasured locations and it is used to convert data from point observations to continuous surfaces. The spatial interpolation techniques are divided into two main groups in terms of concern the application of geostatistical methods and deterministic methods. The degree of similarity between nearby places is used in deterministic interpolation algorithms. They do not account for the spatial relationship between data points and do not give information about the accuracy of the estimates. In contrast, the spatial autocorrelation of the measured points is used in geostatistical interpolation techniques, which provides numerous indicators of the accuracy of the estimates.

There are various interpolation techniques such as Inverse Distance Weight (IDW), Radial basis functions, simple Kriging, etc. (Antonakos and Lambrakis, 2021) In this thesis, IDW was used to calculate the water level measurements of the points at unknown locations and to obtain a surface. IDW is one of the most well-known and widely used deterministic local interpolation techniques and it is named local since the predictions are calculated in a small set of neighboring points. The IDW interpolation principle assumes that the measured values nearest to the predicted location have a stronger impact on the predicted value than those farther away. IDW is an exact interpolator, meaning that the maximum and minimum values of the prediction cannot differ from the values in the dataset. To calculate the predicted values, IDW uses the equation below:

$$\hat{Z}(s_0) = \sum_{i=1}^{N} \lambda_i Z(s_i) \tag{4.8}$$

where $\hat{Z}(s_0)$ is the value to predict for location s_0; N is the number of measured sample points surrounding the prediction location, λ_i are the weights given to each measured point and $Z_{(s)}$ is the observed value at the location s.

The equation used to determine the weights is as follows:

$$\lambda = d_{i0}{}^{-p} \sum_{i=1}^{N} d_{i0}{}^{-p} \tag{4.9}$$

and

$$\sum_{i=1}^{N} \lambda_i = 1 \tag{4.10}$$

where d_{i0} is the distance between the prediction location, s_0, and each of the measured locations, s_i; and p is a power parameter that affects how the measured location's value is weighted on the prediction location's value.

Two factors mainly affect the result of the IDW, these are the value of the power parameter and the neighborhood size, respectively. The choice of these two main parameters is often arbitrary. The most popular p option is 2, which is generally accepted as the default value in many spatial interpolation software. However, the power parameter can be selected based on the mean absolute error minimization, resulting in optimal IDW. In this study, water loads calculated for the three different grid sizes $0.25° \times 0.25°$, $0.5° \times 0.5°$, and $1° \times 1°$ respectively. The reason for using different grid sizes is to examine the compatibility of these estimated displacement values calculated from water load with the GPS station. While the reality of change is not reflected in very small grid sizes, it would also not be correct to interpret the change in the area by using grid sizes that are too large. In addition, considering that the significant relationship between river gauges and GPS stations is in a 100 km buffer (see Section 4.2.1), it was found correct to use a maximum grid size of 1 for this study. The model results obtained using different grid sized water loads are discussed in the Chapter 5.

4.4   Forward Modelling

Forward modeling is used to investigate the physical relationship between vertical displacements and mass loads on Earth's surfaces. There are numerous methods for calculating the deflection of the surface produced by hydrological loading that relies on an Earth model with a certain shape and form assumption (Becker and Bevis, 2004). For example, Boussinesq (1885) solved a point load problem, whereas Lamb (1902) and Terazawa (1916) used Fourier–Bessel transforms to solve the problem of uniform pressure applied within a circular boundary. Using Boussinesq's potential technique, Love (1929) explored the circular or disc load problem. It is also created a new type of loading problem: uniform pressure applied to a rectangular area of the surface. In this study, the response of a uniform elastic half-space to a rectangular load, which is ideal for use with a load extending over a small area is used (Steckler et al., 2010).

The core objective of the uniform elastic half-space model is to calculate the stress and displacement fields caused by applied loads on elastic media that cover the three-dimensional spatial region described in cartesian coordinates space. The solutions to the point load on an elastic half-space problem is three dimensional (3D) Green function (influence function) used in the determination of stresses and displacement fields caused in elastic half-space by general load distributions (Ike, 2019). The model considers displacements caused by a uniform pressure, p, applied over a rectangular region defined by $a \leq x \leq a$, $-b \leq y \leq b$ at the surface ($z = 0$) of a semi-infinite solid (Figure 4.9), where z is positive downward and points in the solid have $z > 0$.
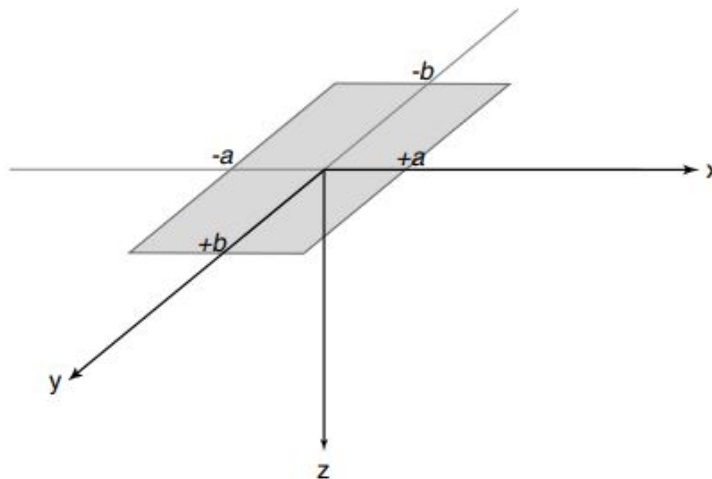
Figure 4.9: Negative correlation between AME4 station and corresponding river gauges within the buffer 20km are shown. The station AME4 has only negative correlation.

According to Love (1929), the coordinates of a point within the solid represented by x, y, z and x', y', 0 to be those of a point on the plane boundary and indicate the distance between these points by r where

$$r^2 = \Delta x^2 + \Delta y^2 + \Delta z^2, \tag{4.11}$$

for $\Delta x = x' - x$, $\Delta y = y' - y$ and $r > 0$. The vertical displacement w produced by this applied pressure are given as:

$$w = \frac{1}{4\pi\mu}\left(\frac{\lambda + 2\mu}{\lambda + \mu}V - z\frac{\partial V}{\partial z}\right), \tag{4.12}$$

where λ and μ are the Lame constants,

$$\chi = \int_{-a}^{a}\int_{-b}^{b} p\log(z + r)\,dx'\,dy' \tag{4.13}$$

χ refers to Boussinesq's 3-D logarithmic potential, and

$$V = \int_{-a}^{a}\int_{-b}^{b} pr^{-1}\,dx'\,dy' \tag{4.14}$$

V denotes the Newtonian potential of a surface distribution. For a uniform pressure p, χ and V depend on Δx and Δy. The Lame constants in Equation 4.12 which are λ and μ, derived from two adjustable model parameters: the Young's modulus (E) and the Poisson's ratio (ν) can be derived as:

$$\mu = \frac{E}{2(1 + \nu)} \tag{4.15}$$

and

$$\lambda = \frac{E\nu}{(1 + \nu)(1 - 2\nu)} \tag{4.16}$$

E is always a positive number and can be seen as a measure of stiffness. ν is

unitless and it measures the strain rate. Sensitivity to Poisson's ratio is actually negligible, so in practice only Young's modulus is set and ν is usually set to a standard value 0.25. Young's modulus was varied to find the value that best fit the vertical displacements at the GPS stations.

The more detailed analytical expression of vertical displacement w is defined as:

$$w = \frac{p}{4\pi\mu}\left[\frac{\lambda + 2\mu}{\lambda + \mu}(L_1 - L_2) + z\left\{\tan^{-1}\frac{(a-x)\Delta y}{zr_{10}} + \tan^{-1}\frac{(a+x)\Delta y}{zr_{20}}\right\}\right]_{y'=-b}^{y'=b} \quad (4.17)$$

or

$$w = \frac{p}{4\pi\mu}\left[\frac{\lambda + 2\mu}{\lambda + \mu}(M_1 - M_2) + z\left\{\tan^{-1}\frac{(b-y)\Delta x}{zr_{01}} + \tan^{-1}\frac{(b+y)\Delta x}{zr_{02}}\right\}\right]_{x'=-a}^{x'=a} \quad (4.18)$$

p in Equations 4.17 and 4.18 refers to load magnitude in our case it is column of water thickness h apply a pressure:

$$p = \rho g h \quad (4.19)$$

where ρ is density of water and it equals to 1000 $kg\,m^{-3}$, g refers to gravity with magnitude 9.82 m^{-2} and h is water thickness or it is called water depth.

To calculate the deformation of the earth's crust due to water load by using a uniform elastic half-space model for the thesis study, the code of Becker and Bevis (2004) was used. All the formulas mentioned above can be briefly summarized as: first, the Love numbers are calculated for a particular earth model in this study through flat-earth approximation. It is based on the calculation of the displacements and potential perturbation generated by a point force pressing on the surface of an elastic half-space using the Boussinesq problem. Second, to produce the various Green's functions, the appropriate weighted sums of the Love numbers are totaled. Thus the calculation of the load response is reduced to the evaluation of a convolution integral. As a result, the deformation due to each rectangular load at each observation point is calculated, and the overall deflection at each observation point is derived by adding all contributions (Farrell, 1972). The detailed form of how Equations 4.17 and 4.18 are derived can be found in the paper (Becker and Bevis, 2004). In this part of the thesis, the problem statement about Elastic half-space model is given. The results obtained from the model and the comparison with the GPS data are expressed in Section 5.

Chapter 5

Results and Discussion

Consistency of the deformations derived from forward modeling with the displacement values obtained from the GPS time series was investigated in the last section of the thesis. The agreement between datasets depends on two variables, young's modulus and grid size. In section a, grid size was used to determine water loads using IDW, a spatial interpolation approach, which was then used as input in modeling. Calculations were performed for three different grid of mass point forces in this study: $0.25° \times 0.25°$, $0.5° \times 0.5°$, and $1° \times 1°$. The grid sizes are presented as inputs in the modeling section to see which resolution best explains the significant relationship between water level and distance value. The sensitivity to the Poisson's ratio is actually negligible so that in practice only the Young's modulus is modified and it is usually set to a constant value of 0.25, as is the case in this study. The relation between both the Young's modulus value and deformation can be directly interpreted, since the Young's modulus is a measurement of an elastic body's resistance to deformation. It's also important in the Boussinesq problem for predicting the correct spherical Green's functions for a given load and data distribution.

These two criteria were utilized to make comparisons for the 23 GPS stations used in the study, although only two of them were included here. Consequently, the value of Young's modulus was adjusted (in a range from 30 GPa to 270 GPa) to find the best fit for the vertical displacements at GPS sites LMCN, and MGW3. For selected values of E and grid size 0.5°, Figures 5.1A, 5.2A, 5.3A, and 5.4A demonstrate the differences between computed and observed vertical displacements at the three GPS sites. For each of comparison of the GPS to the computed deflection, the Figures 5.1B, 5.2B, 5.3B, and 5.4B shows RMS values. The plot of RMS values reveals a significant assymetry between Young's modulus and RMS values. This asymetry derives from the fact that the amplitude of a vertical load's deflection takes the form of (Steckler et al., 2010)

$$w = p(1 + \nu)/E[(1 - \nu)f(x, y, z) + zg(x, y, z)] \tag{5.1}$$

yielding

$$w_{z=0} = p(1 - \nu^2)/Ef(x, y, 0) \tag{5.2}$$

where $w_{z=0}$ is the vertical deflection at the surface and w is the vertical displacement, p is the load, ν is Poisson's ratio, E is Young's modulus, and $f(x, y, z)$ and $g(x, y, z)$ are geometric functions characterizing the deflection as a function of location relative to the load, respectively. The deflections fall off as $1/r$, the distance from the load, at large distances from the loads. Becker and Bevis (2004) provide the complete formula for a rectangular region. The deflection is inversely proportional to E in all circumstances. According to Bevis et al. (2005), the deflection is only slightly dependent on ν. Values as low as 0.27 or even 0.30 would only result in a 1% to 3% reduction in E.

The MGW3 station (Figures 5.1 and 5.2) showed an decreasing RMS value curve for the changing E values. The RMS value for different Young's modulus values varied between 3.8 mm and 2.6 mm. The coherence in the model and GPS time series seems to have almost disappeared with the increase in the E value. While both time series show similar displacements for $E = 30$ value, as the E value increases and stiffness increases, the response to displacement due to mass load almost disappears and therefore the time series of model becomes a straight line. The dates of major hurricanes in the MRD are indicated by the black vertical lines. After these big hurricane, while there was a subsidence in the GPS station, as can be seen from the time series, it is possible to see that there is also a downward movement in the estimates made from the model. Unfortunately, the subsidence that the model shows after the hurricane takes place after the GPS due to the time lag between two time series. It cannot be said that the displacement estimation calculated from the model provides a good agreement with the displacement obtained from the GPS station. Only where the Young's modulus value is small is there a consistency.

Figure 5.1: (a) Calculated displacements for various values of Young's modulus (*E*) compared to vertical displacements at the GPS station MGW3 and (b) calculated RMS values between computed and observed vertical displacements. The black vertical lines show the dates of major hurricanes in the MRD.
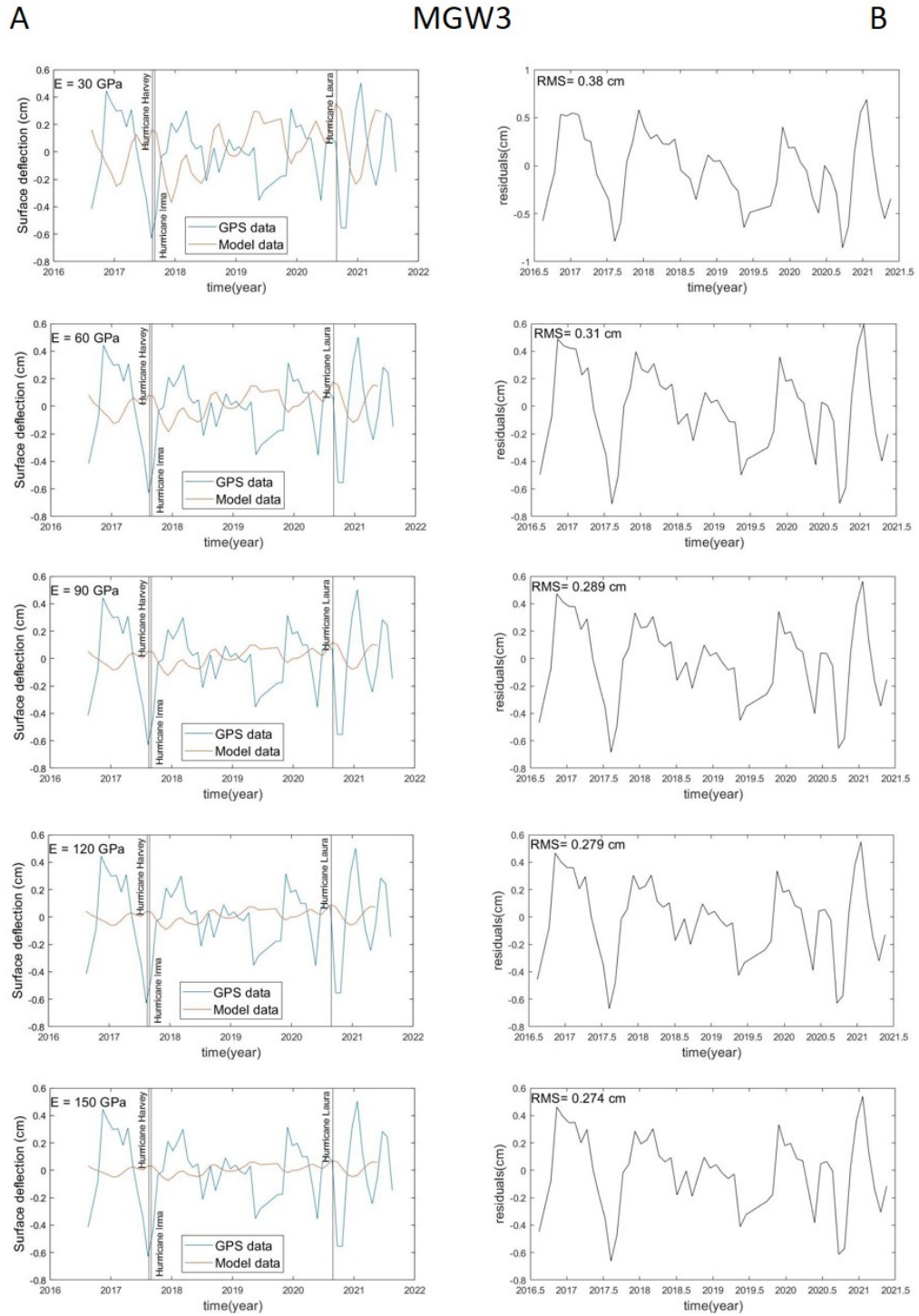
Figure 5.2: (continued)

Figure 5.3: (a) Calculated displacements for various values of Young's modulus (*E*) compared to vertical displacements at the GPS station LMCN and (b) calculated RMS values between computed and observed vertical displacements. The black vertical lines show the dates of major hurricanes in the MRD.
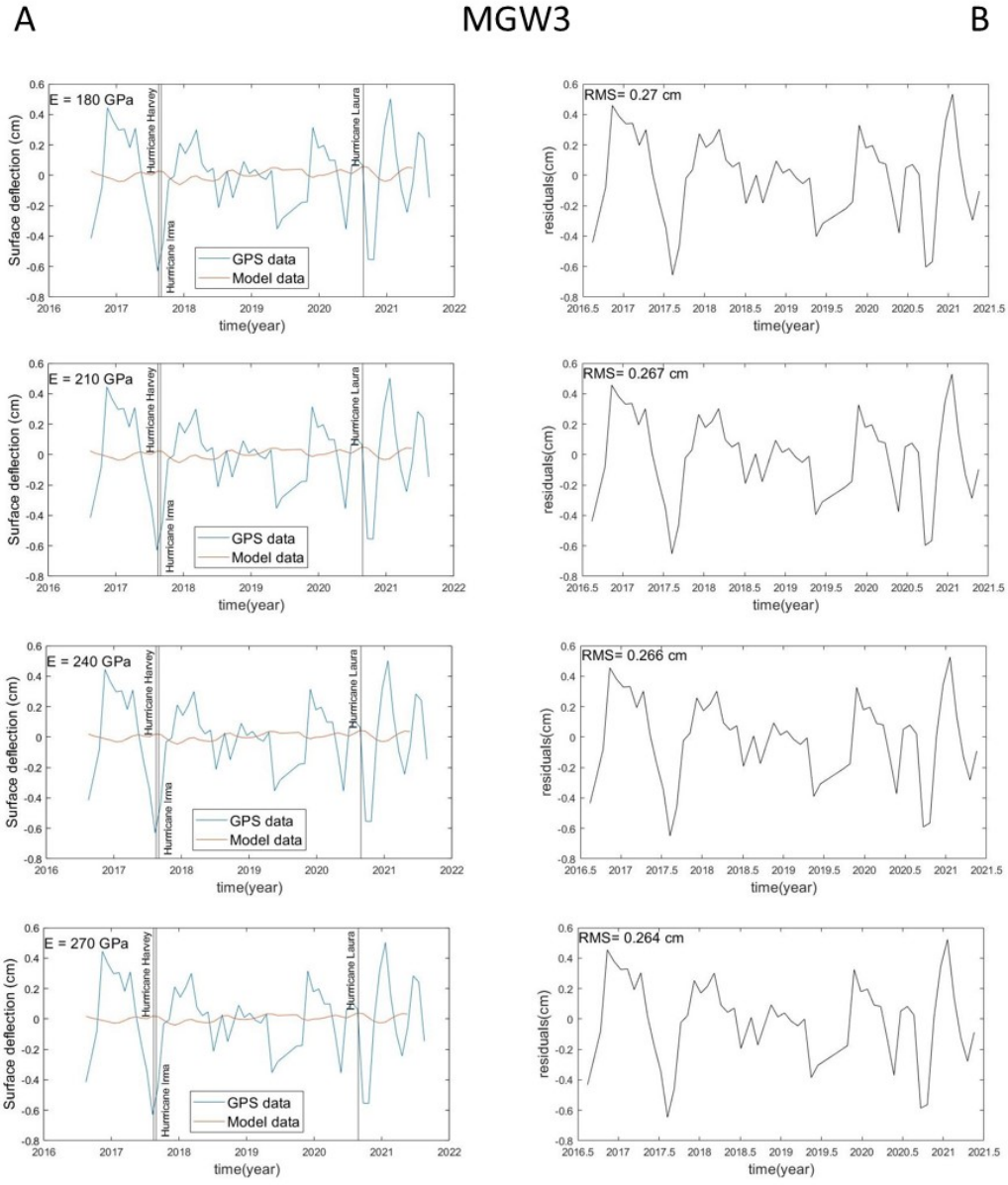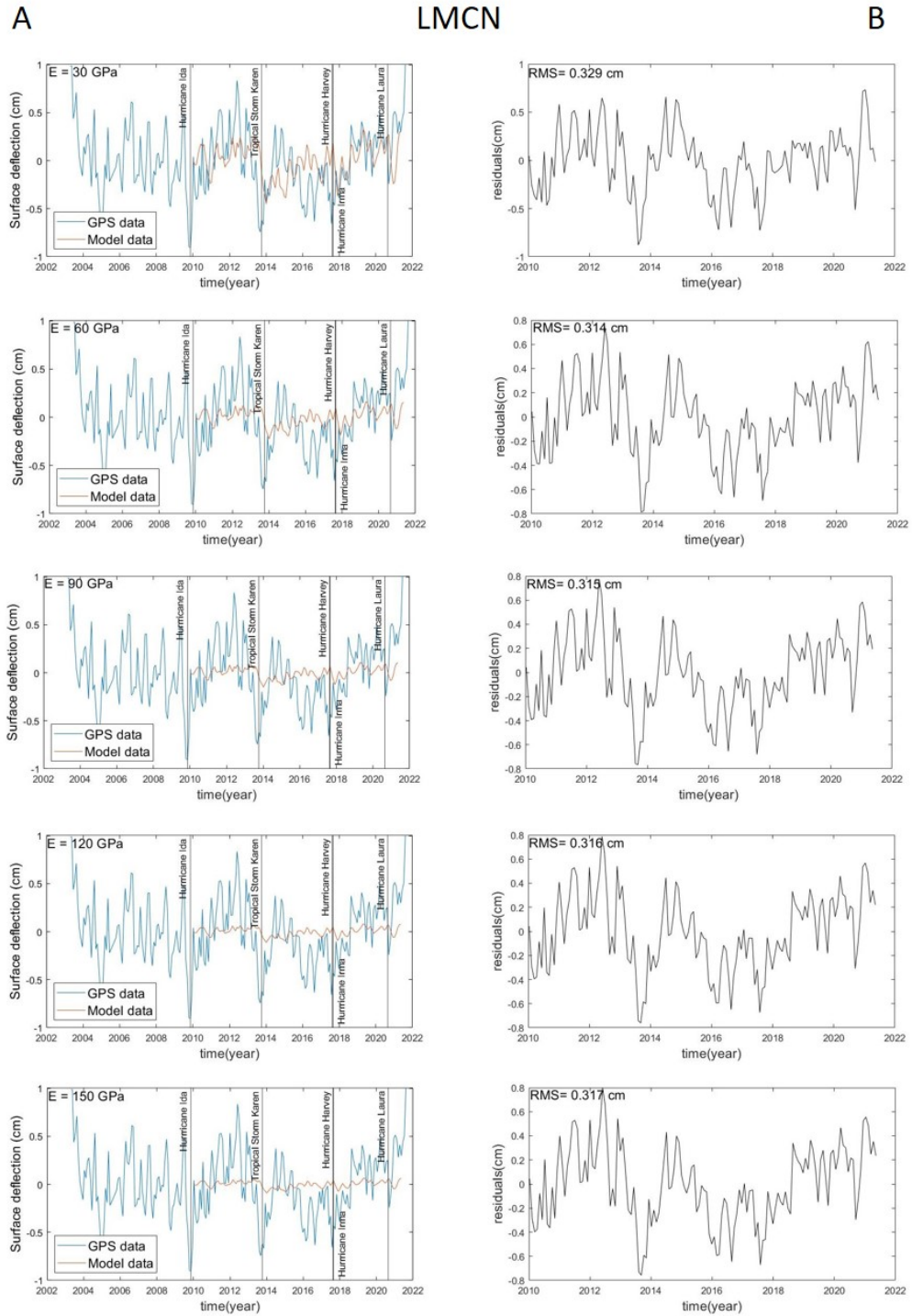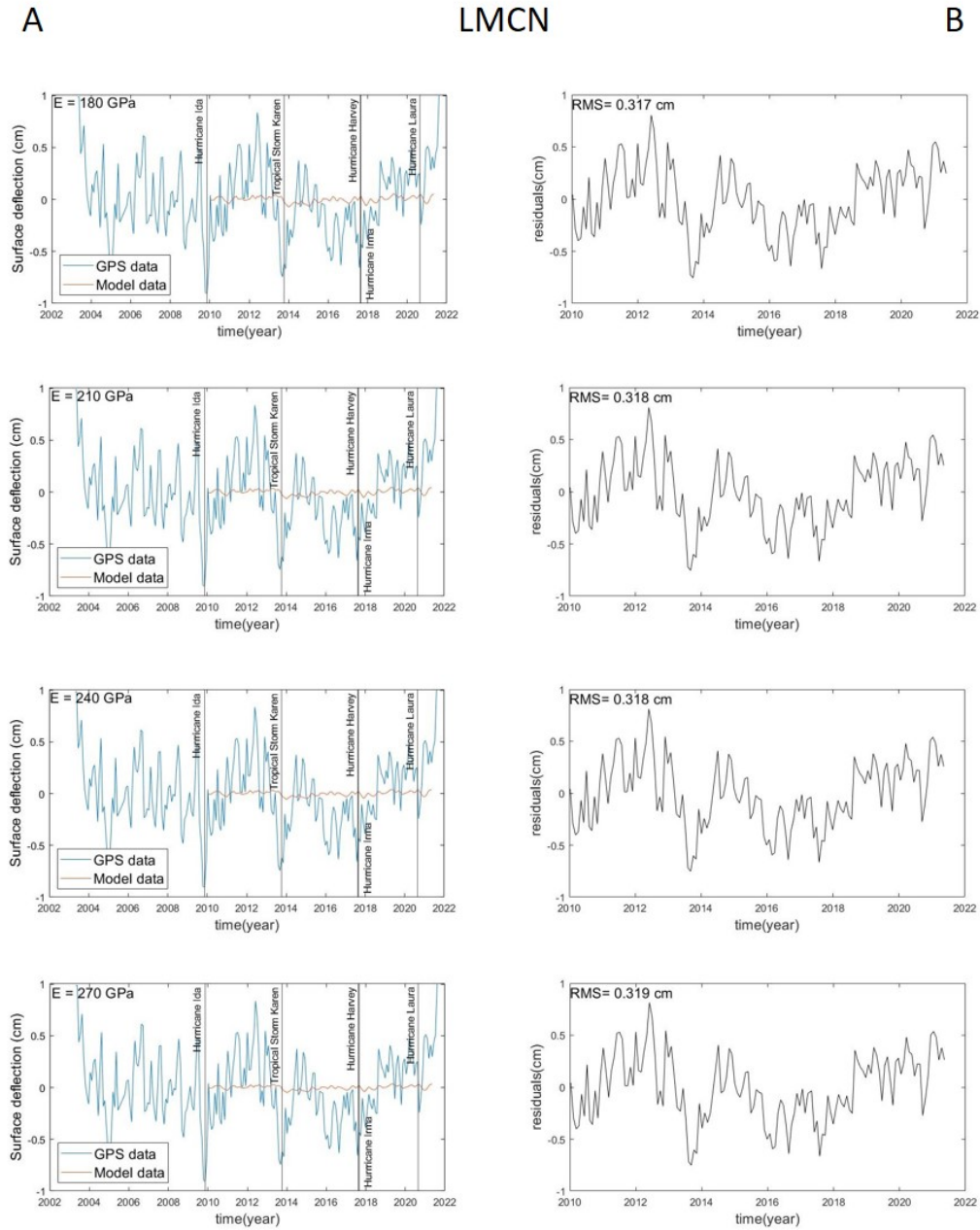
Figure 5.4: (continued)

The station LMCN has the same behavior as the MGW3 station. However, the RMS value starts to increase where it is more than $E = 120$ instead of decreasing continuously. Unlike the MGW3, it has the same variability as the GPS station during the dates of important hurricanes. The RMS value only varies around 3.2 mm. These two stations and all other stations, best match continue until $E = 120$ than the agreement between the two time series disappears.

On the other hand, there is an another criterion for analytical interpretation of results called RMS reduction used for this study. The RMS reduction ratio expressed as a percentage ($\Delta RMS\%$) and the formula is given below;

$$\Delta RMS\% = \frac{RMS(GPS) - RMS(GPS - Model)}{RMS(GPS)} \tag{5.3}$$

Table 3 shows that when Elastic Half-space is used to simulate some of the sites, the RMS values are reduced, demonstrating the possibility of using GPS vertical displacement with the mass loading model for comparison. However, from Table 3 we can see that there are negative RMS attenuation values for most of GPS sites, which means that the RMS values cannot be improved at these sites. In other words, there is a significant phase mismatch between the GPS vertical displacements and the model calculated displacements. However, the most positive RMS reduction value was reached by modeling using 0.5 grid for this study. Thus, these values are given in the table.

Table 5.1: The RMS reduction ratio in percent when estimating GPS vertical displacements with model best fitting value E=120. Stations start with those with a positive RMS reduction value and continue with those with a negative value.

Site Name	$\Delta RMS\%$	Site Name	$\Delta RMS\%$
ENG5	34.7%	LANP	-2.7%
LACC	33%	INRI	-3.9%
ENG6	26.7%	MRY2	-4.5%
BVHS	20.4%	LABL	-4.6%
LMCN	9.9%	SBCH	-4.9%
LABV	4.9%	MGW2	-6.3%
GRIS	2.9%	LAGM	-9%
LAFR	0.6%	AME4	-9.8%
LHJI	0.4%	MGW3	-11%
LABR	-1.2%	MGW1	-12.9%
LAHO	-1.4%	HOUM	-15.8%
FSHS	-2.2%		

The variation of RMS reduction value with Young's modulus is shown in Figure 5.5 and 5.6 for GPS stations ENG5 and LACC that give the best positive values. As it can be clearly seen from both figures, while there is a continuous increase in the range where the E value is up to 120 GPa, there is no remarkable change after this value and the relationship between them turns into a straight line. Therefore, the RMS reduction values of the stations for $E = 120$ are given in the table (Table 5.1) above.
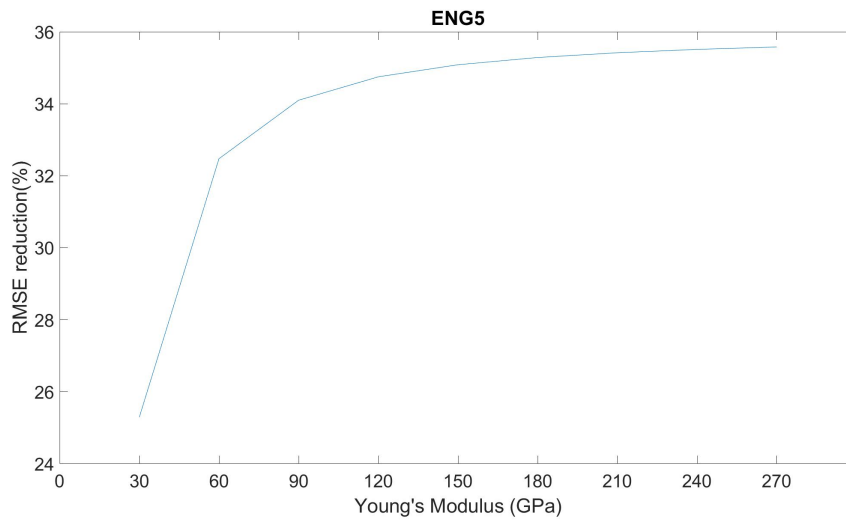

Figure 5.5: The variation of RMS reduction value with Young's modulus is shown for station ENG5.
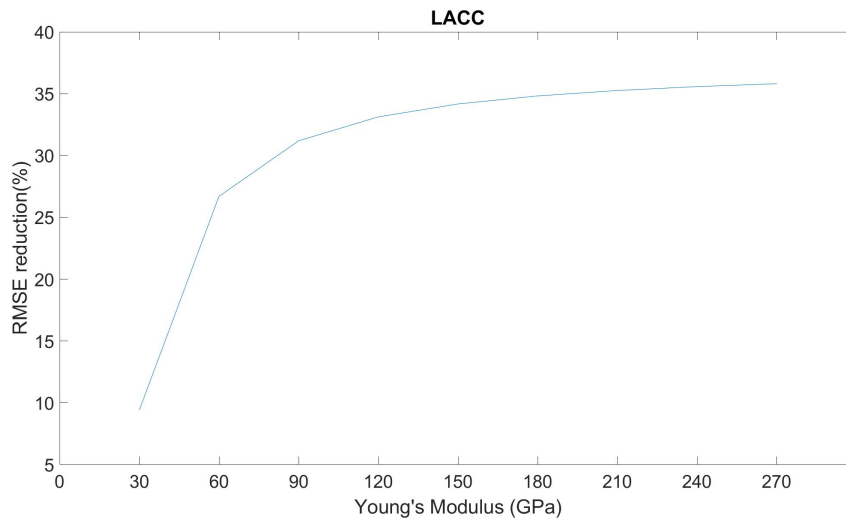

Figure 5.6: The variation of RMS reduction value with Young's modulus is shown for station LACC.

It is currently difficult to quantify errors in the mass loading model. Therefore, in this section, the errors, shortcomings and limitations of the study are discussed and the points that need improvement in future studies are presented. Earth deformation caused by surface mass loading depends on many factors, including the specific geodetic network, the quality of the geodetic data, the computational techniques, the accuracy and spatial distribution of the load model, and the sensitivity to structure (Martens et al., 2016).

The majority of non-linear changes observed in GPS time series are most likely due to geophysical phenomena (e.g., continental drift inthe horizontal coordinates and glacial isostatic adjustmentin the vertical component) rather than analysis errors. The low correlation suggests that local processes or site-specific analytical errors may be dominating GPS deformation estimations at some sites. However, the lack of correlation could possibly be due to errors in GPS analysis. Since, effect of non tidal ocean and atmospheric loading not considered for correcting GPS time series in this study. The impact of these corrections along the coast is relatively high. Therefore, making these corrections will be of great importance in describing the relationship between the model and the GPS, and the displacement estimated from the model will be more accurate. Also, the latest strategies known to reduce spurious signals on quasi-annual and semi-annual periods are suggested to be used in GPS analysis (Fu et al., 2015).

The bias in estimating the water load solely based on river gages has several consequences (Steckler et al., 2010). First, during the beginning of the rainy season, the amount of stored water is likely overestimated. This will result in a change in the results toward higher Young's modulus values. Second, it causes a shift in the water load's timing. As a result of the time lag, the predicted deflection curve frequently falls and rises before the observed GPS deflection. The longer wavelength mismatch is caused by this difference during the rising and falling limbs for higher values of E; the cyclicity in the misfit is shifted relative to the water loading.

Another reason may be that the IDW interpolation technique was weak for this study. Kriging method, which is a geostatistical interpolation technique, is used instead of IDW interpolation to calculate water load. Since IDW is based on the extent of similarity between nearby points, they do not consider the spatial correlation between data points and do not provide a measure of the accuracy of the estimates. On the contrary, the Kriging technique makes use of the spatial autocorrelation of the measured points and provides several indicators of the accuracy of the estimates (Antonakos and Lambrakis, 2021).

Finally, the estimation of deformation computed by assuming a perfectly elastic Earth model and Green's functions, describing the surface deformation response

47

to a point load, considered for an elastic homogeneous half-space model in this thesis. An elastic half-space model is commonly assumed to be a suitable first-order approximation for modeling surface displacements caused by surface loading (e.g., Bevis et al., (2005); Grapenthin et al., (2006); Bettinelli et al., (2008); Steckler et al., (2010)). The half-space model, according to Farrell (1972), fails to adjust the amplitude of the seasonal fluctuations of the vertical and horizontal components at the same time. This indicates that the two components are extremely sensitive to the location of the load. The phase has also been underestimated. However, the study states that this phase difference can cause problems in horizontal displacements, in changes in the vertical component, the predicted displacements are approximately in phase with the observations. The study emphasizes the importance of modeling deformation using a realistic model of the elastic Earth structure. Moreover, the Young's modulus needed to approximate the correct Green's function using a Boussinesq's approximation from the modeling of vertical displacement. It is typically of the order of 110 to 190 GPa as found in other studies (Bevis et al.,(2005); Steckler et al., (2010))

The study still has many limitations that provide warnings about the results. In the conclusion part, all necessary concerns are explained as it is of great importance in developing the results from the model in future research.

Chapter 6

Conclusions

Sea-level rise, coastline erosion, and wetland loss are all caused by coastal subsidence, posing a threat to coastal dwellers. This is notably obvious in the Mississippi Delta, which was destroyed by Hurricane Katrina in 2005 in the southern United States (Törnqvist et al., 2008). The loss of flood-protecting wetlands is considered to be a major contributor to the massive flood damage. The reasons of coastal Louisiana subsidence, which have been attributed to sources as diverse as shallow compaction and deep crustal processes, are still debated. Subsidence rates are currently estimated to differ by several orders of magnitude. Despite the necessity of understanding the impact of surface mass loadings, no comprehensive investigation of the corresponding vertical land motion variability in the continent's broadscale area has been conducted. The GPS and, less commonly because to their complex infrastructure and high costs, Doppler Orbitography and Radiopositioning Integrated by Satellite (DORIS), Satellite Laser Ranging (SLR), and Very Long Baseline Interferometry are currently the principal approaches for measuring the VLM. Nevertheless, the geodetic approaches discussed above are insufficient by themselves to recover certain local loadings associated with mass transport processes in continental hydrology. Thus, the Gravity Recovery and Climate Experiment (GRACE) and loading models have become useful datasets for modeling VLM caused by various surface mass variations.

GRACE's application in low-lying areas and floodplains, where surface runoff and floods are key drivers to water storage variability, continues to be a significant problem. For this study, water level data from Mississippi Delta river measurements is used to produce a spatial surface load. The vertical displacement is then estimated using the elastic half-space model and compared to the GPS time series. To make a valid comparison, the time series carefully refined to remove outliers and correct for the offsets, and then spatial interpolation method IDW used to estimate water level in unmeasured locations and convert data from point observations to continuous surfaces.

The results show that the deformation caused by the water loads calculated from the model provides aggregation for some stations with the displacements in the GPS time series. RMS values differ according to grid resolution and young's modulus value. The best combination for station MGW3 has 2.7 mm RMS value. RMS reduction values differ from -50% to -4% according to young's modulus. The station LMCN has 3.1 mm RMS value and their RMS reduction values changes between 6% to 10%. It can be clearly seen that in the big hurricane and tornado dates model and GPS results have agreement on subsidence. However, the model is not enough to explain this subsidence properly for all stations. The reasons for this are that there are still jumps in the time series or that the flat earth approximation used was not sufficient for modeling. Another reason may be errors due to the spatial interpolation technique used to calculate water loads. Using alternative earth model assumption, experimenting with different interpolation approaches, and correcting the offset-related errors of GPS time series in detail will all be of great importance in enhancing the results derived from the model in future investigations.

Bibliography

Allison, M., Yuill, B., Törnqvist, T., Amelung, F., Dixon, T., Erkens, G., Stuurman, R., Jones, C., Milne, G., Steckler, M., et al. (2016). Global risks and research priorities for coastal subsidence. *Eos (Washington, DC)*, *97* (cit. on p. 19).

Antonakos, A., & Lambrakis, N. (2021). Spatial interpolation for the distribution of groundwater level in an area of complex geology using widely available gis tools. *Environmental Processes*, *8*(3), 993–1026 (cit. on pp. 33, 47).

Argus, D. F., Fu, Y., & Landerer, F. W. (2014). Seasonal variation in total water storage in california inferred from gps observations of vertical land motion. *Geophysical Research Letters*, *41*(6), 1971–1980.

Becker, J. M., & Bevis, M. (2004). Love's problem. *Geophysical Journal International*, *156*(2), 171–178 (cit. on pp. 35, 37).

Bettinelli, P., Avouac, J.-P., Flouzat, M., Bollinger, L., Ramillien, G., Rajaure, S., & Sapkota, S. (2008). Seasonal variations of seismicity and geodetic strain in the himalaya induced by surface hydrology. *Earth and Planetary Science Letters*, *266*(3-4), 332–344.

Blewitt, G., Hammond, W. C., & Kreemer, C. (2018). Harnessing the gps data explosion for interdisciplinary science. *Eos*, *99*(10.1029), 485 (cit. on p. 17).

Blum, M. D., & Roberts, H. H. (2009). Drowning of the mississippi delta due to insufficient sediment supply and global sea-level rise. *Nature Geoscience*, *2*(7), 488–491 (cit. on pp. 9–11).

Borsa, A. A., Agnew, D. C., & Cayan, D. R. (2014). Ongoing drought-induced uplift in the western united states. *Science*, *345*(6204), 1587–1590.

Coleman, J. M., Roberts, H. H., & Stone, G. W. (1998). Mississippi river delta: An overview. *Journal of Coastal Research*, *14*(3), 699–716. http://www.jstor.org/stable/4298830 (cit. on p. 5)

Day, J. W., Cable, J. E., Lane, R. R., & Kemp, G. P. (2016). Sediment deposition at the caernarvon crevasse during the great mississippi flood of 1927: Implications for coastal restoration. *Water*, *8*(2), 38 (cit. on p. 10).

Day Jr, J. W., Boesch, D. F., Clairain, E. J., Kemp, G. P., Laska, S. B., Mitsch, W. J., Orth, K., Mashriqui, H., Reed, D. J., Shabman, L., et al. (2007). Restoration of the mississippi delta: Lessons from hurricanes katrina and rita. *science*, *315*(5819), 1679–1684 (cit. on pp. 6, 9).

Farrell, W. (1972). Deformation of the earth by surface loads. *Reviews of Geophysics*, *10*(3), 761–797 (cit. on p. 37).

Fok, H. S., Zhou, L., Liu, Y., Ma, Z., & Chen, Y. (2019). Upstream gps vertical displacement and its standardization for mekong river basin surface runoff reconstruction and estimation. *Remote Sensing*, *12*(1), 18.

Fok, H. S., Zhou, L., Liu, Y., Tenzer, R., Ma, Z., & Zou, F. (2020). Water balance standardization approach for reconstructing runoff using gps at the basin upstream. *Remote Sensing*, *12*(11), 1767.

Fu, Y., Argus, D. F., & Landerer, F. W. (2015). Gps as an independent measurement to estimate terrestrial water storage variations in washington and oregon. *Journal of Geophysical Research: Solid Earth*, *120*(1), 552–566 (cit. on p. 47).

Gahalaut, V., Yadav, R. K., Sreejith, K., Gahalaut, K., Bürgmann, R., Agrawal, R., Sati, S., & Bansal, A. (2017). Insar and gps measurements of crustal deformation due to seasonal loading of tehri reservoir in garhwal himalaya, india. *Geophysical Journal International*, *209*(1), 425–433.

Grapenthin, R., Sigmundsson, F., Geirsson, H., Arnadóttir, T., & Pinel, V. (2006). Icelandic rhythmics: Annual modulation of land elevation and plate spreading by snow load. *Geophysical Research Letters*, *33*(24).

Hiatt, M., Snedden, G., Day, J. W., Rohli, R. V., Nyman, J. A., Lane, R., & Sharp, L. A. (2019). Drivers and impacts of water level fluctuations in the mississippi river delta: Implications for delta restoration. *Estuarine, Coastal and Shelf Science*, *224*, 117–137.

Ike, C. C. (2019). Love stress function method for solving axisymmetric elasticity problems of the elastic halfspace. *Electronic Journal of Geotechnical Engineering*, *24*(3), 663–706 (cit. on p. 35).

Jankowski, K. L., Törnqvist, T. E., & Fernandes, A. M. (2017). Vulnerability of louisiana's coastal wetlands to present-day rates of relative sea-level rise. *Nature Communications*, *8*(1), 1–7 (cit. on pp. 1, 9).

Ji, K. H., & Herring, T. A. (2012). Correlation between changes in groundwater levels and surface deformation from gps measurements in the san gabriel valley, california. *Geophysical Research Letters*, *39*(1).

Li, J., Miyashita, K., Kato, T., & Miyazaki, S. (2000). Gps time series modeling by autoregressive moving average method: Application to the crustal deformation in central japan. *Earth, planets and space*, *52*(3), 155–162 (cit. on p. 26).

Li, Z., Yue, J., Hu, J., Xiang, Y., Chen, J., & Bian, Y. (2018). Effect of surface mass loading on geodetic gps observations. *Applied Sciences*, *8*(10), 1851.

Martens, H. R., Rivera, L., Simons, M., & Ito, T. (2016). The sensitivity of surface mass loading displacement response to perturbations in the elastic structure of the crust and mantle. *Journal of Geophysical Research: Solid Earth*, *121*(5), 3911–3938 (cit. on p. 47).

Materna, K., Feng, L., Lindsey, E. O., Hill, E. M., Ahsan, A., Alam, A. K., Oo, K. M., Than, O., Aung, T., Khaing, S. N., et al. (2021). Gnss characterization of hydrological loading in south and southeast asia. *Geophysical Journal International*, *224*(3), 1742–1752.

Montazeri, S. (2013). Gps time series analysis (cit. on pp. 21, 22).

Nicholls, R. J., & Small, C. (2002). Improved estimates of coastal population and exposure to hazards released. *Eos, Transactions American Geophysical Union*, *83*(28), 301–305 (cit. on pp. 1, 2).

Nikolaidis, R. (2002). *Observation of geodetic and seismic deformation with the global positioning system*. University of California, San Diego. (Cit. on pp. 22, 23).

Ochieng, K. (2018). *Comparison of deformation and surface water level time series from different locations at the port of rotterdam* (Doctoral dissertation). Van Hall Larenstein. (Cit. on p. 26).

Olson, K., & Suski, C. (2021). Mississippi river delta: Land subsidence and coastal erosion. *Open Journal of Soil Science*, *11*(03), 139 (cit. on pp. 2, 5).

Penland, S., & Ramsey, K. E. (1990). Relative sea-level rise in louisiana and the gulf of mexico: 1908-1988. *Journal of Coastal Research*, 323–342.

Protection, L. C., & (LACAPRA), R. A. (2012). Louisiana's comprehensive master plan for a sustainable coast.

Puskas, C. M., Meertens, C. M., & Phillips, D. (2017). Hydrologic loading model displacements from the national and global data assimilation systems (nldas and gldas). *UNAVCO Geodetic Data Service Group* (cit. on p. 33).

Roth, D. (2010). Louisiana hurricane history (cit. on pp. 10, 15).

Shirzaei, M., Freymueller, J., Törnqvist, T. E., Galloway, D. L., Dura, T., & Minderhoud, P. S. (2021). Measuring, modelling and projecting coastal land subsidence. *Nature Reviews Earth & Environment*, *2*(1), 40–58 (cit. on p. 26).

Steckler, M. S., Nooner, S. L., Akhter, S. H., Chowdhury, S. K., Bettadpur, S., Seeber, L., & Kogan, M. G. (2010). Modeling earth deformation from monsoonal flooding in bangladesh using hydrographic, gps, and gravity recovery and climate experiment (grace) data. *Journal of Geophysical Research: Solid Earth*, *115*(B8) (cit. on pp. 35, 39, 47).

Törnqvist, T. E., Wallace, D. J., Storms, J. E., Wallinga, J., Van Dam, R. L., Blaauw, M., Derksen, M. S., Klerks, C. J., Meijneken, C., & Snijders, E. (2008). Mississippi delta subsidence primarily caused by compaction of holocene strata. *Nature Geoscience*, *1*(3), 173–176 (cit. on p. 49).

Van Oldenborgh, G. J., Van Der Wiel, K., Sebastian, A., Singh, R., Arrighi, J., Otto, F., Haustein, K., Li, S., Vecchi, G., & Cullen, H. (2017). Attribution of extreme rainfall from hurricane harvey, august 2017. *Environmental Research Letters*, *12*(12), 124009.

Wang, L., Chen, C., Du, J., & Wang, T. (2017). Detecting seasonal and long-term vertical displacement in the north china plain using grace and gps. *Hydrology and Earth System Sciences, 21*(6), 2905–2922.

Wolstencroft, M., Shen, Z., Törnqvist, T. E., Milne, G. A., & Kulp, M. (2014). Understanding subsidence in the mississippi delta region due to sediment, ice, and ocean loading: Insights from geophysical modeling. *Journal of Geophysical Research: Solid Earth, 119*(4), 3838–3856.

Wu, X., Heflin, M. B., Ivins, E. R., Argus, D. F., & Webb, F. H. (2003). Large-scale global surface mass variations inferred from gps measurements of load-induced deformation. *Geophysical research letters, 30*(14).

Appendix A

GPS Time Series Correction
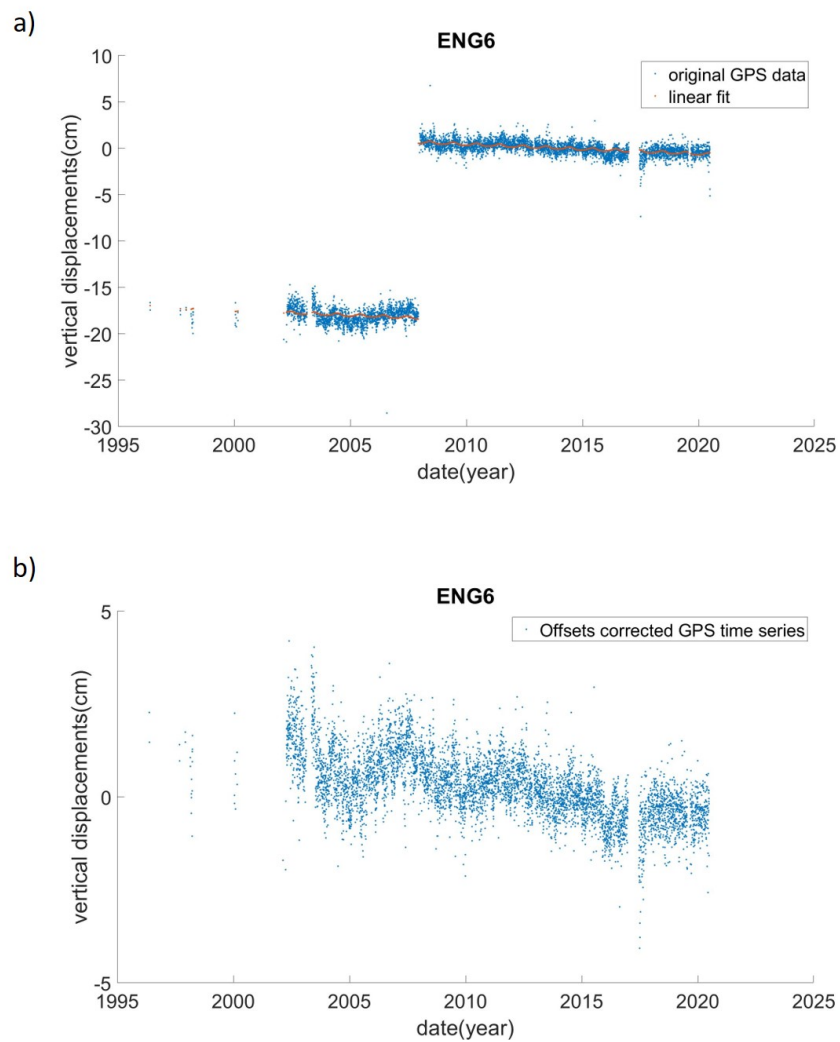
Figure A.1: (a) The original GPS time series and its linear trend are shown as orange line, (b) the corrected time series after removing outliers

a)
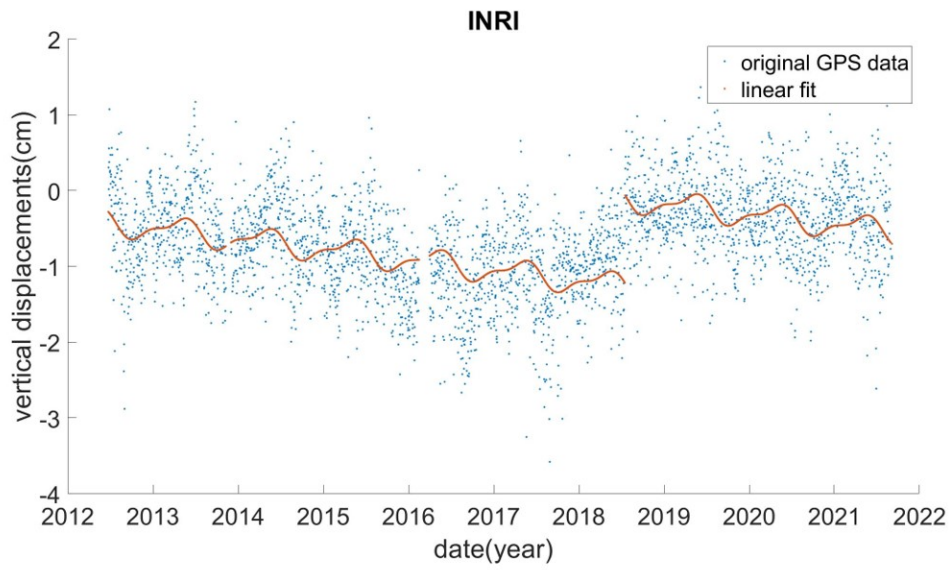
b)
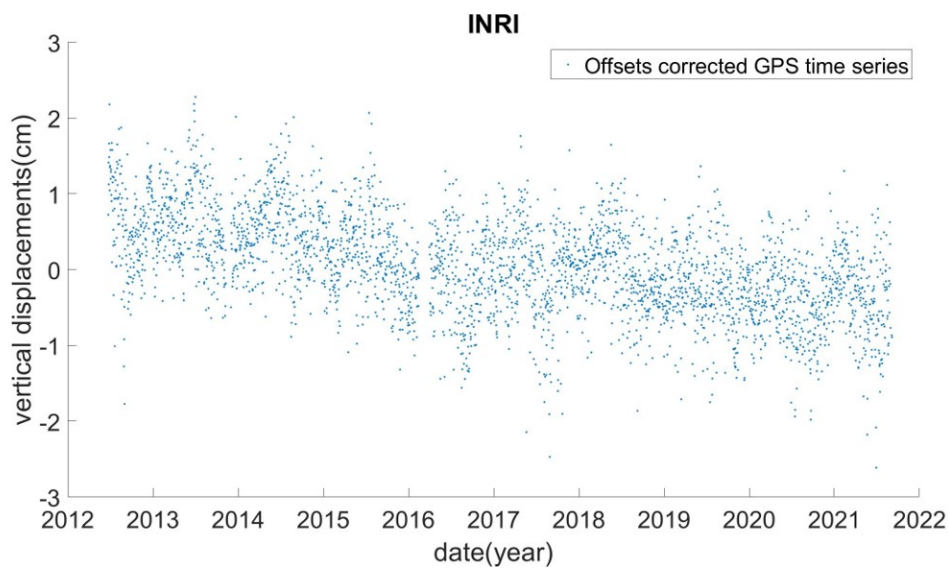
Figure A.2: (a) The original GPS time series and its linear trend are shown as orange line, (b) the corrected time series after removing outliers

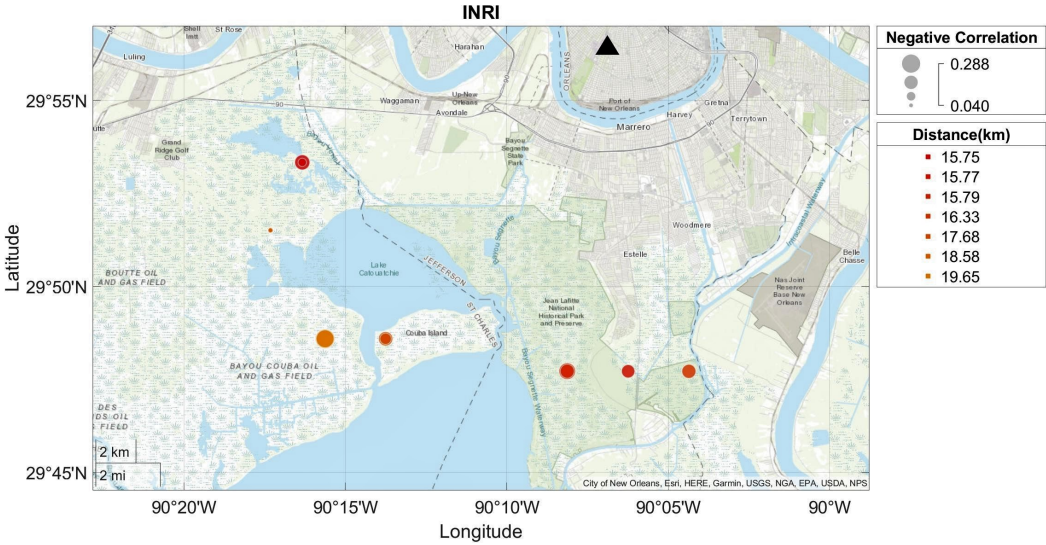# Appendix B

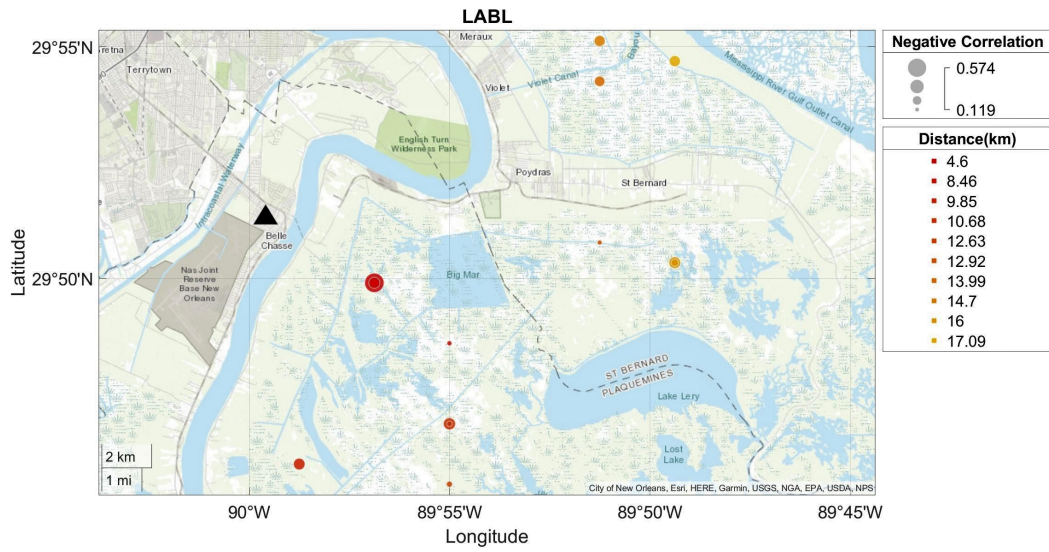**Relationship between water level and VLM**

Figure B.1: Negative correlation between INRI station and corresponding river gauges within the buffer 20km are shown with bubbles. The black triangle represent location of the GPS station
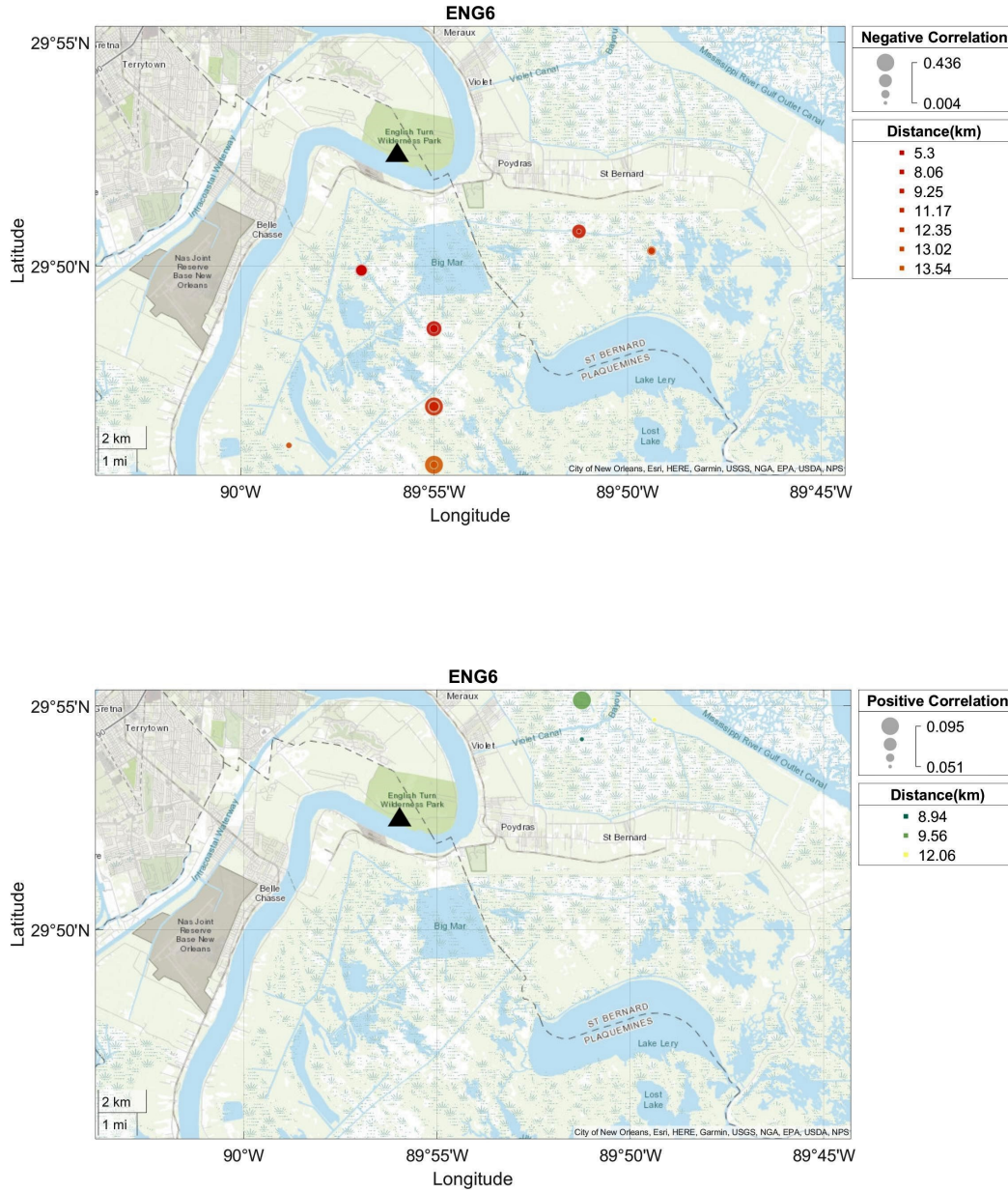
Figure B.2: Positive and negative correlation between ENG6 station and corresponding river gauges within the buffer 20km are shown with bubbles. The black triangle represent location of the GPS station

Figure B.3: Negative correlation between LABL station and corresponding river gauges within the buffer 20km are shown with bubbles. The black triangle represent location of the GPS station
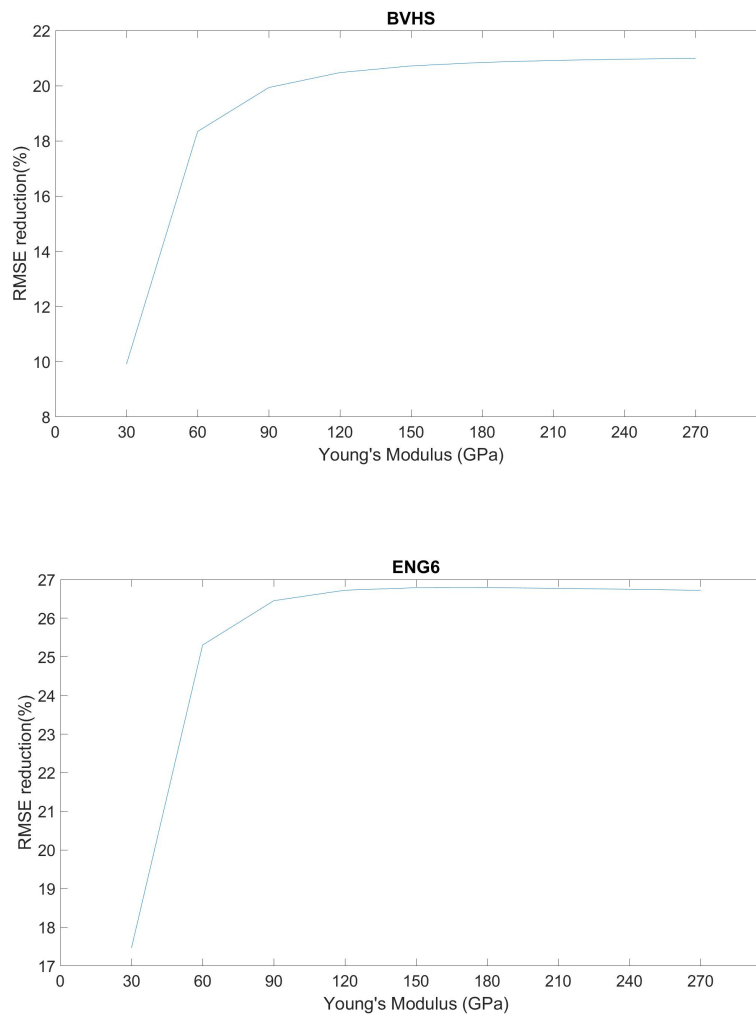
Appendix C

GPS vs Model Comparison

Figure C.1: The variation of RMS reduction value with Young's modulus is shown for station BVHS and ENG6
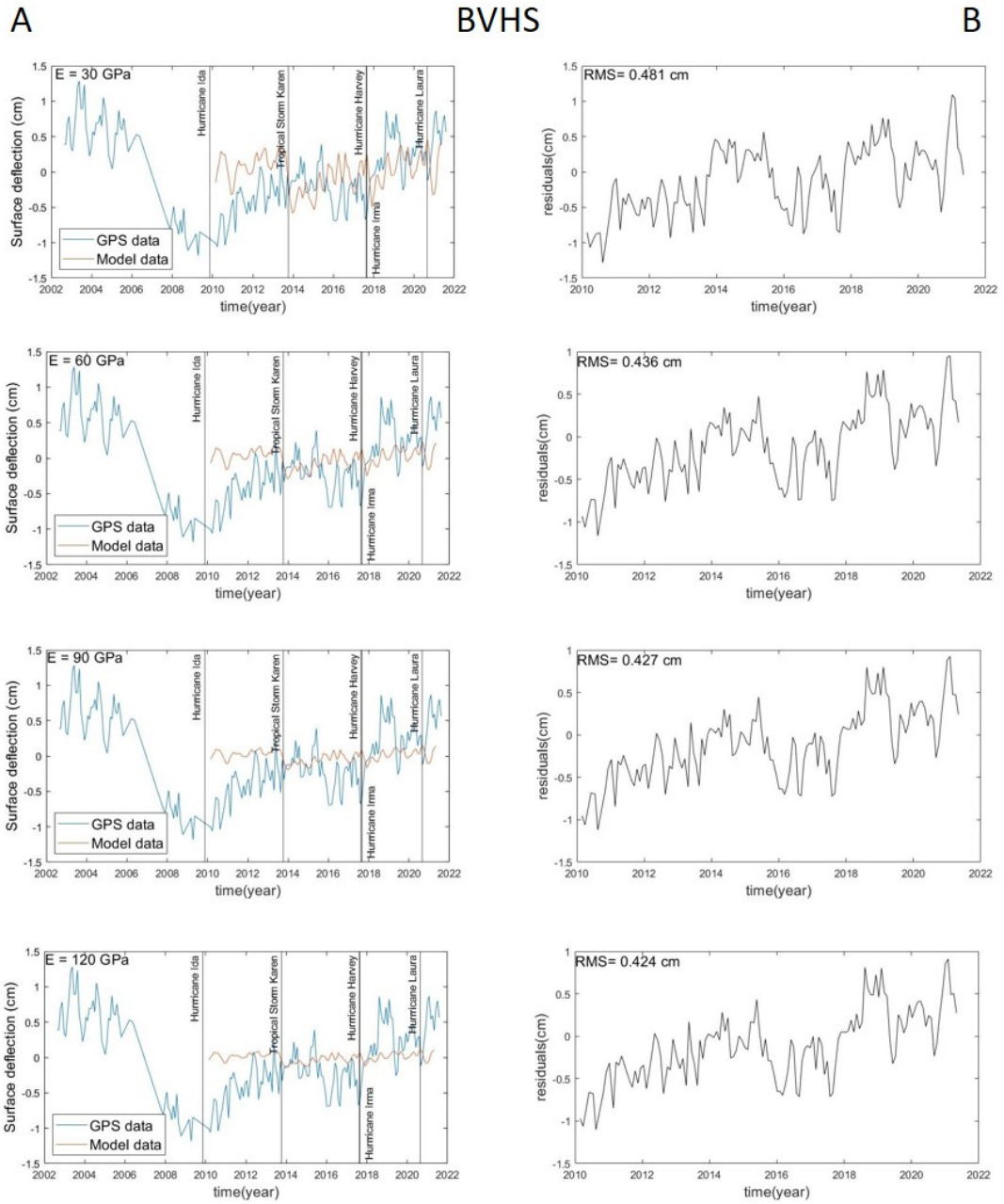
Figure C.2: (a) Calculated displacements for various values of Young's modulus (*E*) compared to vertical displacements at the GPS station BVHS and (b) calculated RMS values between computed and observed vertical displacements. The black vertical lines show the dates of major hurricanes in the MRD.
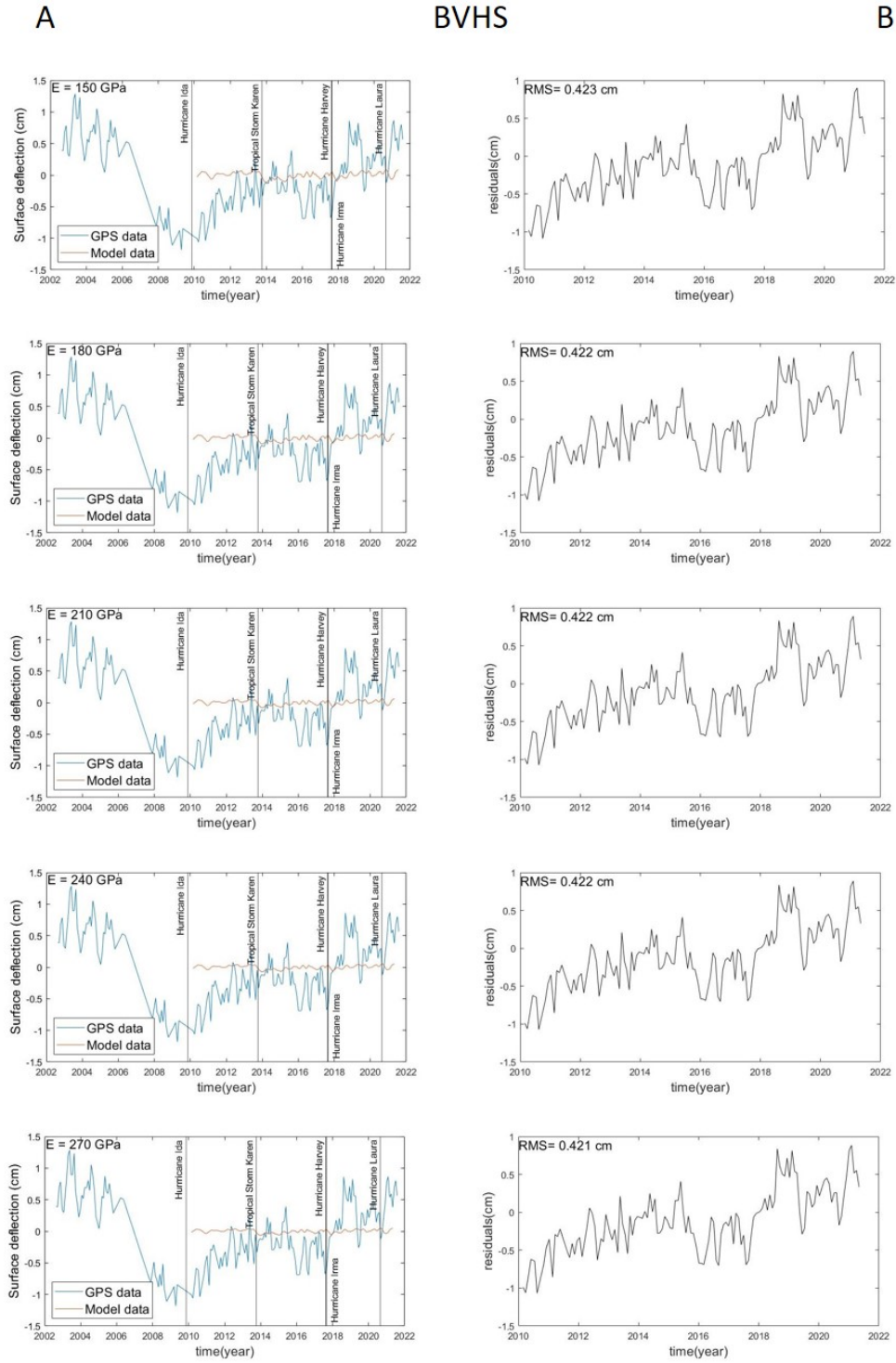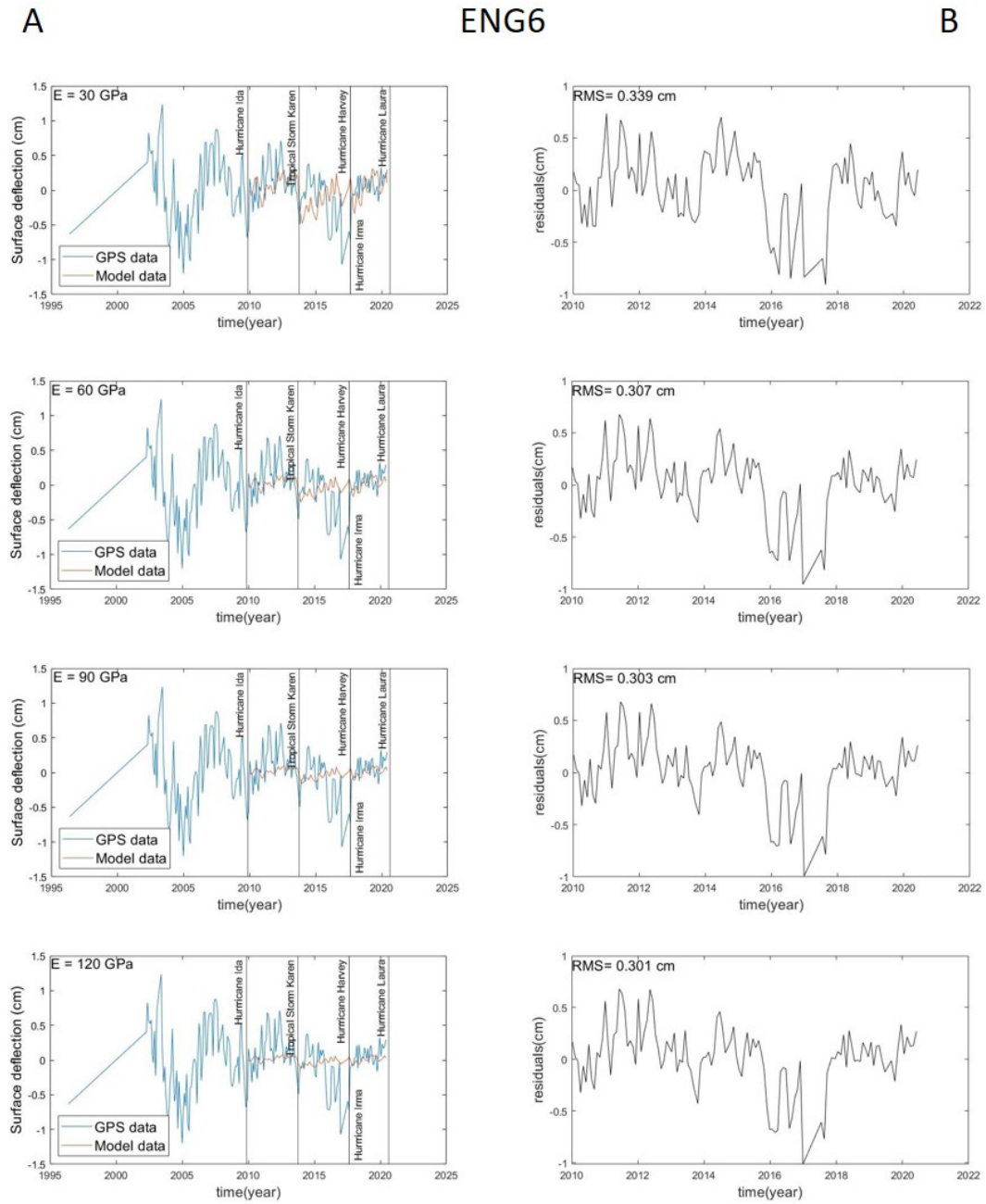
Figure C.3: (continued)

Figure C.4: (a) Calculated displacements for various values of Young's modulus (E) compared to vertical displacements at the GPS station ENG6 and (b) calculated RMS values between computed and observed vertical displacements. The black vertical lines show the dates of major hurricanes in the MRD.
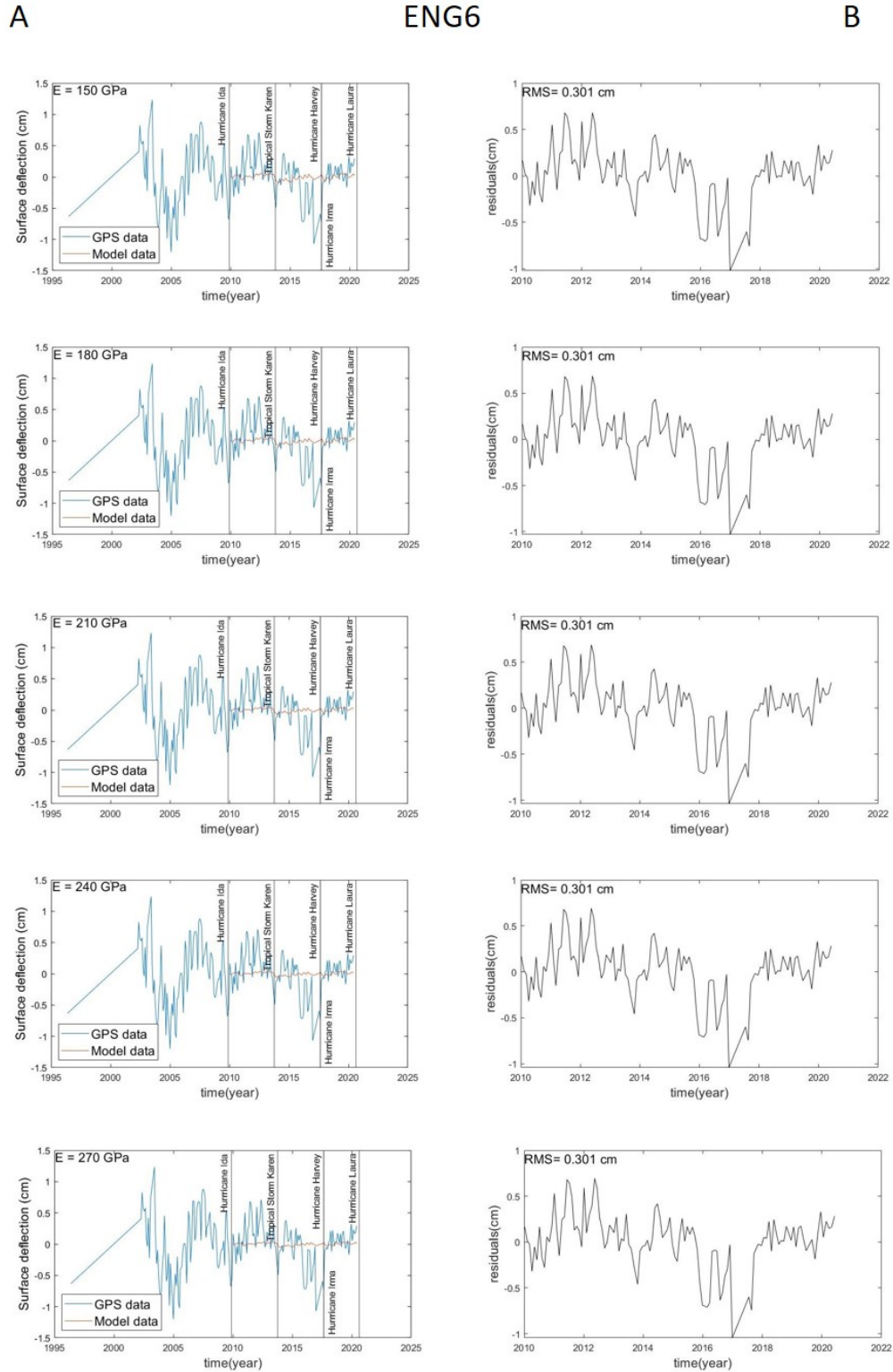
Figure C.5: (continued)

64